THE UNIVERSITY OF CALGARY

THE EFFECT OF WETTABILITY AND PORE GEOMETRY ON THREE PHASE FLUID DISPLACEMENT IN POROUS MEDIA

BY

V. WILLIAM TANG KONG

A THESIS

SUBMITTED TO THE FACULTY OF GRADUATE STUDIES

IN PARTIAL FULFILLMENT OF THE REQUIREMENTS FOR THE

DEGREE OF

MASTER OF SCIENCE

DEPARTMENT OF GEOLOGY AND GEOPHYSICS

CALGARY, ALBERTA

APRIL, 1988

ISBN 0-315-42548-2

THE UNIVERSITY OF CALGARY

FACULTY OF GRADUATE STUDIES

The undersigned certify that they have read, and recommend to the Faculty of Graduate studies for acceptance, a thesis entitled, " The Effect of Wettability and Pore Geometry on Three Phase Fluid Displacement in Porous Media " submitted by V. William Tang Kong in partial fulfillment of the requirements for the degree of Master of Science.

N.C. Wardlaw

Supervisor, Dr. N.C. Wardlaw,
Geology and Geophysics

Dr. T.A. Oliver,
Geology and Geophysics

A.A. Levinson

Dr. A.A. Levinson,
Geology and Geophysics

J. Novosad

Dr. J. Novosad,
Petroleum Recovery Institute

Date : 88/04/27

Abstract

Hydrocarbon miscible flooding is expected to become the major enhanced oil recovery method for many Alberta oil fields. Many of the conventional light to medium gravity crude oil reservoirs in Alberta have or are rapidly approaching the mature stage of production, leaving behind significant residual oil volumes.

A major drawback to miscible processes is the fingering of low viscosity, highly mobile solvent into the oil bank, bypassing oil and giving poor sweep efficiencies. A common means of reducing viscous fingering in a reservoir is to inject water alternately with the chase gas that follows the solvent bank (WAG process). The chase gas and water are immiscible. Water, gas and oil interfaces cause a resistance to fluid flow due to contact angle hysteresis and interface curvature distortion, known as the "Jamin effect".

A laboratory study has been undertaken to investigate the magnitude of this resistance under conditions of differing wettability and pore geometry. A series of experiments performed in capillary tubes of constant radius and cross-section determined that the resistance to flow is a function of the number of interfaces present within the capillary and that a higher mobilization pressure is required for oil-wet conditions as compared with equivalent water-wet systems (on the order of 7 to 12 times greater). Furthermore, mobilization pressures are due to contact angle hysteresis, i.e. the difference between the cosines of the advancing and receding contact angles.

A transparent glass micromodel of pores and throats (converging-diverging system) was constructed by a photo imaging and chemical etching

technique to simulate a two-dimensional porous medium. Mobilization pressures within the micromodel are influenced by wettability, pore geometry and bubble size and position. The distortion of bubbles as they pass from bulges (pores) to constrictions (throats) generates a greater magnitude of resistance to flow than that caused by contact angle hysteresis, and increases as aspect ratio (pore-to-throat size) increases. The wetting and nonwetting phases assume characteristic configurations for water-wet and oil-wet conditions which results in different mobilization pressures. Also, intermediately wetted ($\theta \sim 90°$) systems are capable of sustaining finite pressures depending on the position of the interfaces in the pore-throat.

The results obtained from experimental work provide valuable insight into the microscopic displacement of oil in the presence of an immiscible gas phase.

Acknowledgements

The author thanks his supervisor, Dr. N.C. Wardlaw, for suggesting this study; for his excellent guidance, support, encouragement and inexhaustible patience during the course of this study.

In addition, many thanks are extended to Mr. M. McKellar, Research Associate, for his invaluable advice and assistance during all phases of this thesis. The author also wishes to acknowledge R. Larush for providing photographic services. D. Steffes and B. McNamara provided stimulating discussions which were helpful in developing this study.

Many plaudits are extended to all those individuals on the "Fifth Floor", past and present, who made working there so enjoyable. To my friends : H. Abercrombie, J. Bloch, T. Chow, J. Lee, C. McMechan, C. Nahnybida and M. Shevalier, all the best. Thank You.

Table of Contents

Approval Page ii

Abstract iii

Acknowledgements v

Table of Contents vi

List of Tables viii

List of Figures xi

List of Plates xiii

Nomenclature xiv

Chapter 1 Background 1

1.1 General Statement 1

1.2 Fluid and rock interaction 2

1.3 Wettability and Contact Angle Hysteresis 4

1.4 Effect of Pore Geometry on Ganglia Trapping and Mobilization 12

Chapter 2 Materials and Fluid Properties 16

2.1 General Statement 16

2.2 Fluid properties and methods of testing 16

2.3 Design of glass micromodels 19

2.4 Fabrication of the glass micromodel 25

2.5 Geometry of the micromodel 27

Chapter 3 Capillary Tube Experiments 35

3.1 Description of Apparatus 35

3.2 Experimental Procedure 38

3.3 Experimental Data 40
Chapter 4 Glass Micromodel Experiments. 57
4.1 Description of Apparatus 57
4.2 Experimental Procedure 58
4.3 Experimental Data 64
Chapter 5 Discussion 82
5.1 Discussion of Capillary Tube Results. 82
5.2 Discussion of Glass Micromodel Results 88
5.3 Comparison and Significance of Results 94
5.4 Discussion of Error 94
Chapter 6 Conclusions 97
6.1 General Statement 97
6.2 Application to WAG process and immiscible flooding 99
6.3 Recommendations for Future Work. 101
References 102
Appendices 105
A.1 Derivation of equations for mobilization pressure in capillary tubes 106
A.2 Determination of contact angles from photographs 107
A.3 Analysis of Error. 109

List of Tables

2.1 Fluid Densities measured for hexadecane, distilled water and air (Temp. = 22.5 °C) 18

2.2 Surface tension measurement for hexadecane/air using the drop-volume (drop-weight) technique (Temp. = 23.1°C) 20

2.3 Surface tension measurement for distilled water/air using the drop-volume (drop-weight) technique (Temp. = 23.1°C) 21

2.4 Interfacial tension measurement for hexadecane against distilled water using the drop-volume (drop-weight) technique (Temp. = 23.1°C) 22

2.5 Calibration of the Leitz optical microscope for width and depth of etch measurement 28

2.6 The width (x) and depth of etch (y) of the different elements in the lower (model) plate of the glass micromodel. 30

2.7 The width (x) and depth of etch (y) of the different elements in the upper (cover) plate of the glass micromodel. 31

2.8 The effective diameters of the combined upper and lower pores, and the throats; and the aspect (pore-to-throat size) ratios 32

3.1 Mobilization pressures for air in a water-wet capillary tube, obtained from the critical angle of tilt and the length of the bubble 42

3.2 Mobilization pressures for air in a water-wet capillary tube, obtained from contact angle measurements. 42

3.3 Mobilization pressures for hexadecane in a water-wet capillary tube, obtained from the critical angle of tilt and the length of the bubble 43
3.4 Mobilization pressures for hexadecane in a water-wet capillary tube, obtained from contact angle measurements. 43
3.5 Mobilization pressures for hexadecane/air in a water-wet capillary tube, obtained from the critical angle of tilt and the lengths of the two phases 44
3.6 Mobilization pressures for hexadecane/air in a water-wet capillary tube, obtained from contact angle measurements 44
3.7 Mobilization pressures for air in an oil-wet capillary tube, obtained from buret volume and head of water in reservoir 53
3.8 Mobilization pressures for air in an oil-wet capillary tube, obtained from contact angle measurements 53
3.9 Mobilization pressures for hexadecane in an oil-wet capillary tube, obtained from buret volume and head of water in reservoir 54
3.10 Mobilization pressures for hexadecane in an oil-wet capillary tube, obtained from contact angle measurements 54
3.11 Mobilization pressures for hexadecane/air in an oil-wet capillary tube, obtained from buret volume and head of water in reservoir .. 55
3.12 Mobilization pressures for hexadecane/air in an oil-wet capillary tube, obtained from contact angle measurements 56
4.1 Mobilization pressures for air in a water-wet micromodel, obtained from the head difference between the upstream and downstream water reservoirs 65

4.2 Mobilization pressures for hexadecane in a water-wet micromodel, obtained from the head difference between the upstream and downstream water reservoirs 65
4.3 Mobilization pressures for hexadecane/air in a water-wet micromodel, obtained from the head difference between the upstream and downstream water reservoirs 66
4.4 Mobilization pressures for air in an oil-wet micromodel, obtained from buret volume and head of water in reservoir 73
4.5 Mobilization pressures for hexadecane in an oil-wet micromodel, obtained from buret volume and head of water in reservoir 73
4.6 Mobilization pressures for hexadecane/air in an oil-wet micromodel, obtained from buret volume and head of water in reservoir 74
5.1 A comparison of the water-wet and oil-wet capillary tube systems from the difference of the cosines of the advancing and receding contact angles 86
5.2 A comparison of the water-wet and oil-wet glass micromodel systems from the difference of the cosines of the advancing and receding contact angles 91
5.3 Estimation of the precision of the direct and indirect measurements of mobilization pressures in the capillary tube and glass micromodel experiments (Refer to Appendix A.3 for a listing of the errors estimated for primary measured quantities) 96

List of Figures

1 A typical water-oil-solid system with water having a greater affinity for the rock surface than oil, with a contact angle θ_{ows} (after Craig, 1971) 5

2 Contact angle hysteresis : a) Advancing contact angle resulting from the displacement of non-wetting phase by wetting phase; b) Receding contact angle resulting from the displacement of wetting phase by non-wetting phase 7

3 The configuration of three phases (water, oil and gas) in a cylindrical capillary tube for water-wet conditions. 10

4 The configuration of three phases (water, oil and gas) in a cylindrical capillary tube for oil-wet conditions. 11

5 Configuration of a fluid-fluid interface in a toroidal pore model under different wetting conditions (after Purcell, 1950; and Stegemeier, 1977) 14

6 Cross section of pore and throat from glass micromodel 33

7 Apparatus for measuring mobilization pressure in capillary tube experiments. 37

8 Buoyant pressure acting on an oil-gas bubble in a capillary tube with water-wet conditions. The critical angle of tilt indicates the imminent movement of the bubble up the tube 41

9 Apparatus for measuring mobilization pressure in glass micromodel experiments 59

10 Configuration of displaced phases in a water-wet micromodel system 62
11 Configuration of displaced phases in an oil-wet micromodel system 63
12 Results from capillary tube experiments 83
13 Results from glass micromodel experiments 89
14 Geometric relationship to determine the angle the meniscus makes with the inside wall of a capillary tube of diameter b, with a meniscus height h 108

List of Plates

1 A Capillary tube experiment, water-wet displaced phase is air. 47

1 B Capillary tube experiment, oil-wet displaced phase is air. 47

2 A Capillary tube experiment, water-wet displaced phase is hexadecane. 49

2 B Capillary tube experiment, oil-wet displaced phase is hexadecane. 49

3 A Capillary tube experiment, water-wet displaced phase is hexadecane/air 51

3 B Capillary tube experiment, oil-wet displaced phase is hexadecane/air 51

4 Glass micromodel experiment, water-wet displaced phase is air. 68

5 Glass micromodel experiment, water-wet displaced phase is hexadecane. 70

6 Glass micromodel experiment, water-wet displaced phase is hexadecane/air 72

7 Glass micromodel experiment, water-wet displaced phase is air. 77

8 Glass micromodel experiment, water-wet displaced phase is hexadecane. 79

9 Glass micromodel experiment, oil-wet displaced phase is hexadecane/air 81

Nomenclature

a = capillary constant, m

b = diameter of capillary tube, m

g = acceleration due to gravity, m/s^2

h = height of the meniscus, m;
also head of water required to mobilize bubble, m

J_{ow} = curvature of the interface between oil and water, m^{-1}

J_{dr} = drainage curvature at the leading edge of a blob, m^{-1}

J_{imb} = imbibition curvature at the trailing edge of a blob, m^{-1}

k_e = effective permeability, m^2

k_g = effective permeability to gas, m^2

k_o = effective permeability to oil, m^2

L_g = length of the gas portion of the bubble, m

L_o = length of the oil portion of the bubble, m

M = mobility ratio, dimensionless

N_{Ca} = capillary number, dimensionless

ΔP = mobilization pressure, Pa

$\Delta P/L$ = pressure gradient, Pa/m

P_c = capillary pressure, Pa

P_{dr} = drainage capillary pressure, Pa

P_{imb} = imbibition capillary pressure, Pa

P_o = pressure in the oil phase, Pa

P_w = pressure in the water phase, Pa

P_1 = pressure in fluid one, Pa

P_2 = pressure in fluid two, Pa

r = radius, m

r_p = radius of pore, m

r_t = radius of throat, m

R = radius of curvature of the torus, m

v = apparent velocity calculated using Darcy's equation, m/s

V = volume of water added by buret, L

x = width of etch, m

y = depth of etch, m

α = position of the fluid-fluid interface within the pore, degree

α_c = critical angle of tilt, degree

α_m = position of the fluid-fluid interface of maximum curvature within the pore, degree

β = aspect ratio (pore-to-throat size), dimensionless

δ = difference of cosines ($\cos \theta_R - \cos \theta_A$), dimensionless

ε = ratio of $\delta_{oil\text{-}wet}$ to $\delta_{water\text{-}wet}$, dimensionless

γ = surface or interfacial tension, N/m

γ_{og} = interfacial tension between oil and gas, N/m

γ_{os} = interfacial tension between oil and solid, N/m

γ_{ow} = interfacial tension between oil and water, N/m

γ_{ws} = interfacial tension between water and solid, N/m

θ = contact angle, degree

θ_A = advancing contact angle, degree

θ_E = intrinsic contact angle, degree

θ_R = receding contact angle, degree

θ_{ows} = contact angle in oil water solid system, degree

θ_{Aog} = advancing contact angle at oil gas interface, degree

θ_{Awo} = advancing contact angle at oil water interface, degree

θ_{Rgo} = receding contact angle at oil gas interface, degree

θ_{Row} = receding contact angle at oil water interface, degree

ρ = density, kg/m^3

$\Delta\rho$ = density difference, kg/m^3

ρ_g = density of gas, kg/m^3

ρ_o = density of oil, kg/m^3

ρ_w = density of water, kg/m^3

μ = viscosity of displacing fluid, Pa s

μ_g = viscosity of gas, Pa s

μ_o = viscosity of oil, Pa s

Chapter 1 Background

1.1 General Statement

The efficiency with which hydrocarbons can be recovered by fluid injection is dependent on several variables that can be categorized into three groups: 1) the properties of the rock-pore system: 2) the properties of the fluids flowing in the system; and 3) the forces acting on the system. While considerable emphasis has been given to the study of two phase fluid interaction (i.e. water and oil) in petroleum reservoirs, the investigation of an additional gaseous phase, whether incipient or introduced, and its effects on the multiphase fluid rock-pore system are less well known.

Enhanced oil recovery projects which involve the use of carbon dioxide or hydrocarbon miscible floods introduce solvent banks in order to achieve a reduction in oil viscosity, promote oil swelling and reduce interfacial tension. However, these types of floods encounter the problem of viscous fingering since the injected solvent is less viscous and more mobile than the oil being displaced. Also, the solvent may be less dense which causes additional problems of gravity override. One means of reducing the high mobility ratio is the alternate injection of chase gas and water into the reservoir. This Water-Alternating-Gas (WAG) process was first proposed by Caudle and Dyes (1958) as an effective means of mobility control. Gas has a lower viscosity than solvent, therefore the gas-solvent front is also highly unstable. The objective of the alternate injection process is to reduce the mobility of the chase gas with the more viscous water, thereby reducing the tendency of gas to finger into the solvent bank, and solvent into the oil bank.

The presence of immiscible gas influences the movement of oil through

reservoir rock by altering the physical properties of the oil and occupying the more conductive portions of the pore spaces, leaving the oil and water to the less conductive portions. Moreover, oil mobilization is hindered by the so-called "Jamin effect" (after French physicist J. Jamin), which is the resistance to flow caused by the boundary conditions of detached gas and liquid bubbles confined in small spaces. The "Jamin effect" is caused by both the contact angle hysteresis and the distortion of the interface curvature as the bubble passes through a constriction.

The objective of the present study is to investigate the magnitude of this resistance and its role in aiding mobility control under conditions of different wettability and pore geometry. Experiments were performed in porous media under well controlled conditions in order that wettability and pore geometry could be investigated. A series of experiments in cylindrical capillary tubes examined the effects of wettabilty on mobilization pressures in the absence of pore geometry. A fabricated glass micromodel was used to study the effects of both wettability and pore geometry. The porous media used do not consider the complexities of the reservoir rock-pore system but provide useful information on fluid-fluid interaction at the microscopic level.

1.2 Fluid and rock interaction

Enhanced oil recovery involves the displacement of discontinuous oil ganglia from the pores of rocks in the petroleum reservoir. The two major forces acting on an oil ganglion are the viscous forces and the capillary forces (Shah, 1981). The ratio of the viscous to the capillary forces determines the microscopic displacement efficiency of residual oil and is refered to as the capillary number (N_{Ca}). Under conditions of normal waterflooding, the capillary

number is on the order of 10 E-06 to 10 E-07. Mobilization of residual oil is achieved when the capillary number is increased to around 10 E-03 to 10 E-02. The capillary number can be expressed by the following equation (Melrose and Brandner, 1974).

$$N_{Ca} = (v\mu)/\gamma \qquad \text{(Eqn. 1.1)}$$

where v = the velocity of the displacing fluid
(maximum of 1 to 2 metres per day)

μ = the viscosity of the displacing fluid (for water, around 1 mPa . s)

γ = the interfacial tension between the displaced and displacing fluids
(usually 15 to 30 mN/m for a normal waterflood)

From the above equation, it can be seen that an increase in the capillary number requires either an increase in both the velocity and/or viscosity of displacement or a decrease in the interfacial tension by three or four orders of magnitude. However, an increase in either velocity or viscosity must be accompanied by a large pressure gradient, which in practice cannot be achieved because the fracture pressure of the reservoir rock would be exceeded. Therefore, under practical reservoir conditions, a favorable capillary number can be best achieved by substantially decreasing the interfacial tension at the oil/brine interface (Shah, 1981).

In Darcy's Law, there is a proportionality factor which relates fluid velocity to pressure gradient. This proportionality factor, termed the mobility, is the effective permeability divided by the fluid viscosity (Craig, 1971). The ratio of the mobility of the displacing phase to the mobility of the displaced phase is known as the mobility ratio.

Darcy's Law for horizontal flow is :

$$v = (k_e / \mu)(\Delta P / L) \qquad \text{(Eqn. 1.2)}$$

where v = fluid velocity

(k_e / μ) = mobility of the fluid

$(\Delta P / L)$ = pressure gradient

Mobility ratio is :

$$M = (k_g \mu_o) / (\mu_g k_o) \qquad \text{(Eqn. 1.3)}$$

where M = mobility ratio

k = effective permeability

μ = fluid viscosity

subscripts g and o refer to gas and oil, respectively

It can be seen in the above equation for mobility ratio that, if gas is the displacing fluid and oil the displaced fluid, the mobility ratio will be greater than unity (gas having a lower viscosity than oil and a higher relative permeability). By convention, mobility ratios less than unity are termed "favorable" and those greater than unity as "unfavorable", and refer to the stability of the flood front (Craig, 1971). For an unfavorable mobility ratio, the pressure gradient in the drive fluid (gas) is considerably less than in the driven fluid. This causes the fingering of low viscosity gas into the oil bank, leading to the bypassing of large portions of the reservoir, with the subsequent early breakthrough of gas at the production wells.

1.3 Wettability and contact angle hysteresis

Wettability describes the preference of a fluid to adhere to a solid surface in the presence of another immiscible fluid. The degree of wetting is given by the contact angle. That is, the angle the fluid-fluid interface makes with the solid phase, as measured in the denser fluid (Figure 1). The displacement of nonwetting phase by wetting phase (imbibition) gives the advancing contact

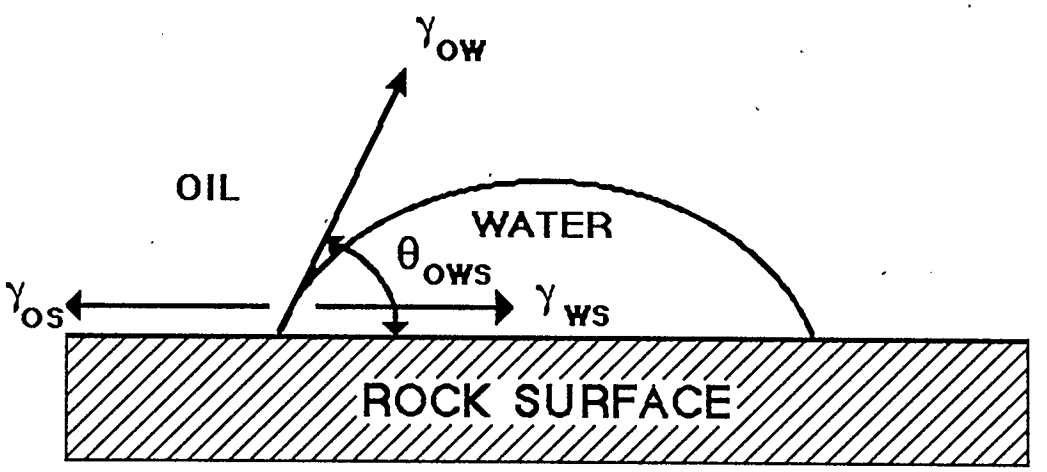

YOUNG EQUATION : $\gamma_{os} = \gamma_{ws} + \gamma_{ow} \cos \theta_{ows}$

Figure 1. A typical water-oil-solid system with water having a greater affinity for the rock surface than oil, with a contact angle θ_{ows} (Craig, 1971).

angle θ_A, and the displacement of wetting phase by nonwetting phase (drainage) gives the receding contact angle θ_R (Figure 2). The intrinsic contact angle, θ_E, represents a system of generally uniform wettability on a smooth, solid surface (Morrow, 1974). In such a system, the advancing contact angle is the same as the receding contact angle, and both θ_A and θ_R are equal to θ_E. This condition of uniform wettability results in zero hysteresis and no pressure can be sustained across the corresponding advancing and receding interfaces if they are located in a cylindrical tube of uniform radius.

The state of static equilibrium for wetting can be described by the Young equation :

$$\gamma_{os} = \gamma_{ws} + \gamma_{ow} \cos \theta_{ows} \quad \text{(for an oil-water-solid system)} \qquad \text{(Eqn. 1.4)}$$

In the above equation, θ_{ows} represents the angle of contact measured through the denser phase, γ represents the interfacial tension between the various phases, the subscripts o, w and s indicate oil, water and solid, respectively. The pressure exerted across an interface between two immiscible fluids is given by the Laplace equation of capillarity :

$$P_o - P_w = \gamma_{ow} J_{ow} \quad \text{(with oil and water as fluids)} \qquad \text{(Eqn. 1.5)}$$

P denotes the pressure in the fluid phases, γ the interfacial tension, J the curvature of the interface, and the subscripts o and w, oil and water, respectively. For a capillary space of uniform diameter and complete wetting (the contact angle being either 0 or 180 degrees), the Laplace equation becomes :

$$P_c = 2\gamma / r \qquad \text{(Eqn. 1.6)}$$

where r is the radius of the capillary and also of the interface.

For incomplete wetting, a term corresponding to the degree of wetting is incorporated into the equation. This new equation is the combined

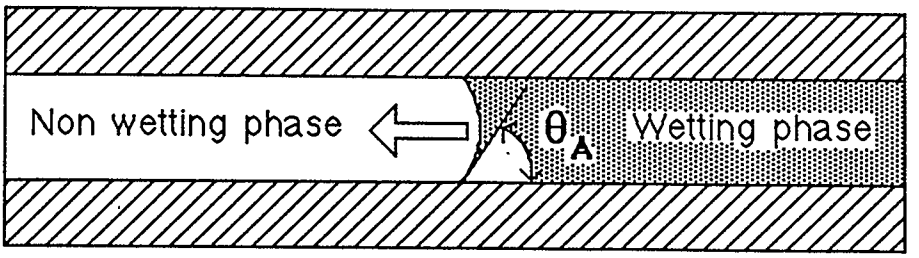

a) Advancing contact angle θ_A

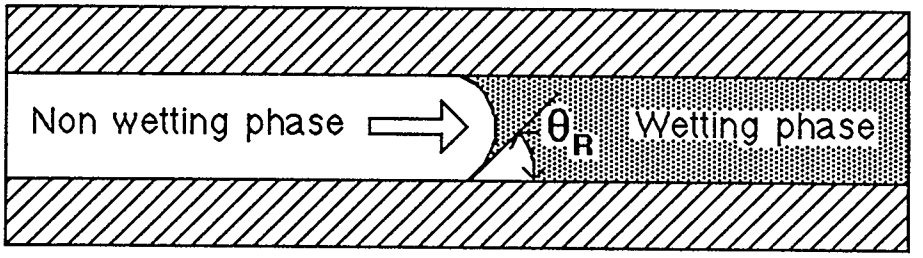

b) Receding contact angle θ_R

Figure 2. Contact angle hysteresis : a) Advancing contact angle resulting from the displacement of non-wetting phase by wetting phase; b) Receding contact angle resulting from the displacement of wetting phase by non-wetting phase.

Young-Laplace equation of capillarity :

$$P_c = (2\gamma \cos\theta) / r \qquad \text{(Eqn. 1.7)}$$

where r is the radius of the capillary but not of the interface, except in the case where $\theta = 0°$.

The Young-Laplace equation can be used to calculate the mobilization pressure of an isolated oil ganglion by determining the maximum pressure across the two oil-brine interfaces. At this position of imminent movement, the ganglion undergoes its maximum distortion, with the greatest hysteresis (largest difference) between advancing and receding contact angles. For an oil blob confined in a water-wet capillary the equation for the mobilization pressure is :

$$\Delta P = P_{dr} - P_{imb} = \gamma (J_{dr} - J_{imb}) \qquad \text{(Eqn. 1.8)}$$

where J denotes the curvature of the interface, γ the interfacial tension between the two phases and subscripts dr and imb, drainage and imbibition, respectively. When contact angle hysteresis and the radii of curvature are taken into consideration, the expression becomes :

$$\Delta P = [2\gamma / r] (\cos\theta_R - \cos\theta_A) \qquad \text{(Eqn. 1.9)}$$

Since the advancing contact angle is always at least as large as the receding contact angle, the cosine of θ_R is greater than the cosine of θ_A. Therefore, the larger the difference between advancing and receding contact angles, the greater the pressure gradient required to mobilize the oil blob.

Similarly, the mobilization pressure for a multiphase fluid-solid system (i.e. oil, brine, gas and solid) can be determined. The configuration of the interfaces between oil and brine changes with differing wettability conditions, i.e. oil-wet or water-wet (the gas phase remains nonwetting with respect to either water or oil).

For a water-wet system with an oil-brine interfacial tension γ_{wo} , an oil-gas interfacial tension γ_{og} , and advancing and receding contact angles associated with the oil-brine interface (θ_{Row} and θ_{Awo}) and the oil-gas interface (θ_{Rgo} and θ_{Aog}) the mobilization pressure is (Figure 3) :

$$\Delta P = \{2 / r\} [\gamma_{wo} (\cos \theta_{Row} - \cos \theta_{Awo}) + \gamma_{og} (\cos \theta_{Rgo} - \cos \theta_{Aog})] \quad \text{(Eqn. 1.10)}$$

For an oil-wet system containing the same fluids and interfaces (Figure 4), the mobilization pressure is :

$$\Delta P = \{2 / r\} [\gamma_{wo} (\cos \theta_{Row} - \cos \theta_{Awo}) + \gamma_{og} (\cos \theta_{Rgo} - \cos \theta_{Aog})] \quad \text{(Eqn. 1.11)}$$

The equations for the mobilization pressures under water-wet and oil-wet conditions for a cylindrical capillary tube are identical. For the derivation of these equations, refer to Figures 3 and 4, and Appendix A.1. Since gas is the nonwetting phase in the presence of oil and water, and the oil-gas interfacial tension is less than the oil-water interfacial tension, the gas phase is separated from the water by oil under both water-wet and oil-wet conditions.

Now, consider a simple porous medium with spheroid-shaped pores and narrow constricted throats. For a blob of oil in such a water-wetted medium, the position of maximum mobilization pressure occurs when the leading edge of the blob, where oil displaces water, is located at the narrowest point of the throat (r_t). In addition, the trailing edge of the blob, where water displaces oil, is located at the widest part of the pore body, whose dimension is r_p. The pressure difference across the blob which is necessary to mobilize it is proportional to the difference in drainage and imbibition capillary pressures, P_{dr} and P_{imb} (Chatzis and Morrow, 1984) :

$$\Delta P = P_{dr} - P_{imb} = \gamma (J_{dr} - J_{imb}) \quad \text{(Eqn. 1.8)}$$

where J denotes the curvature of the interface, γ the interfacial tension between the two phases and subscripts dr and imb, drainage and imbibition,

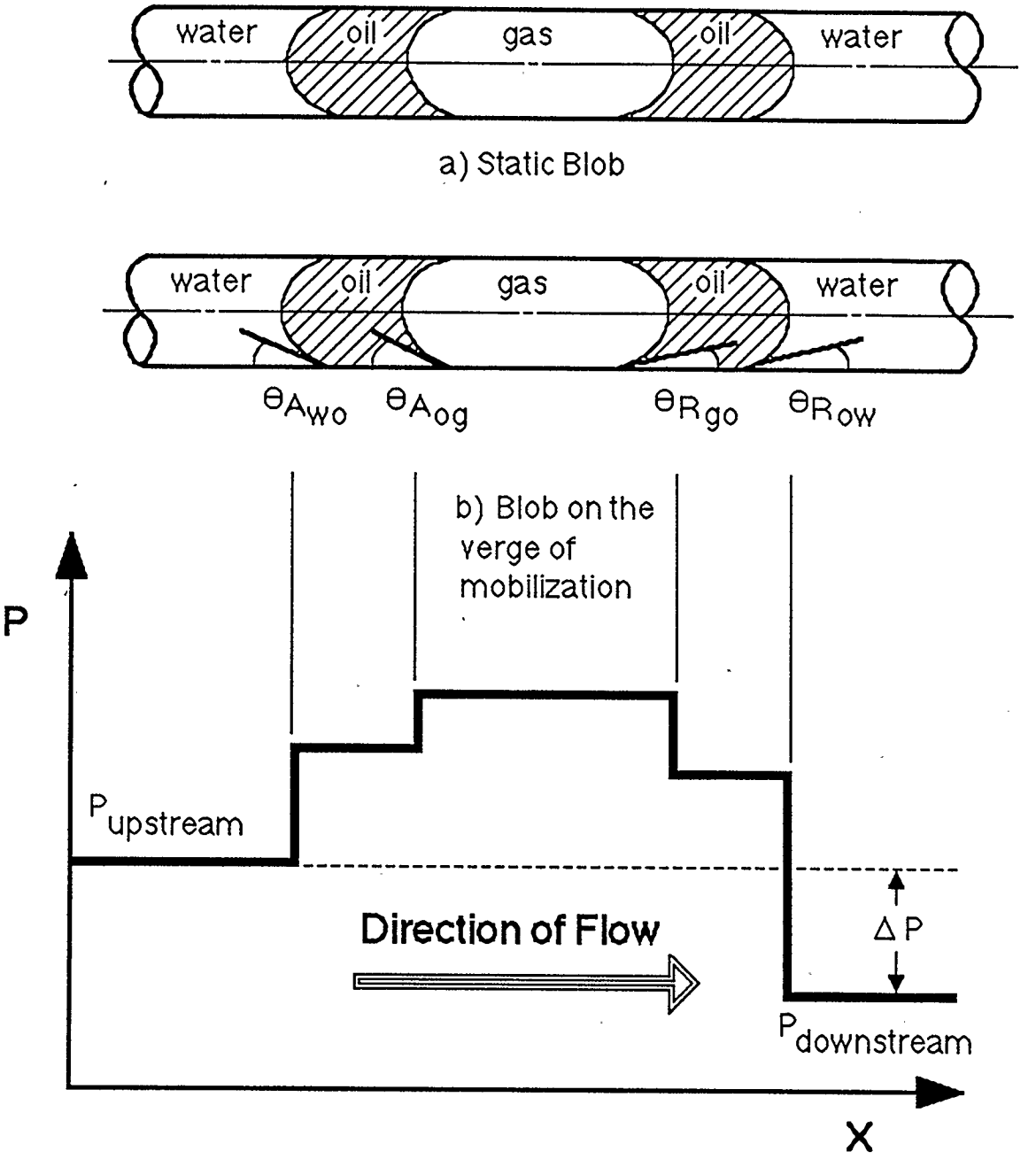

c) Schematic of pressure changes across water-oil and oil-gas interfaces, and mobilization pressure (ΔP)

Figure 3. The configuration of three phases (water, oil and gas) in a cylindrical capillary tube for water-wet conditions.

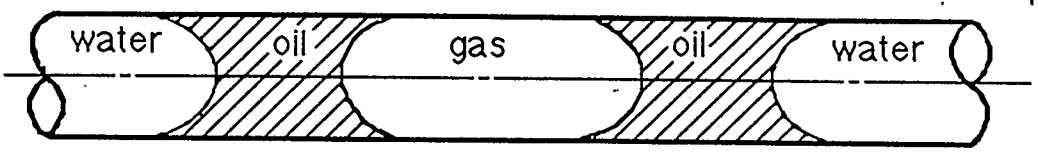

a) Static Blob

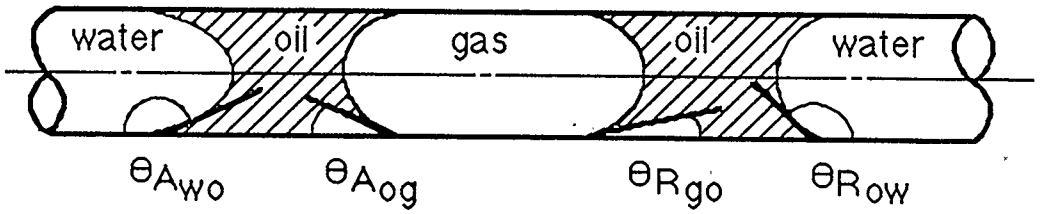

b) Blob on the verge of mobilization

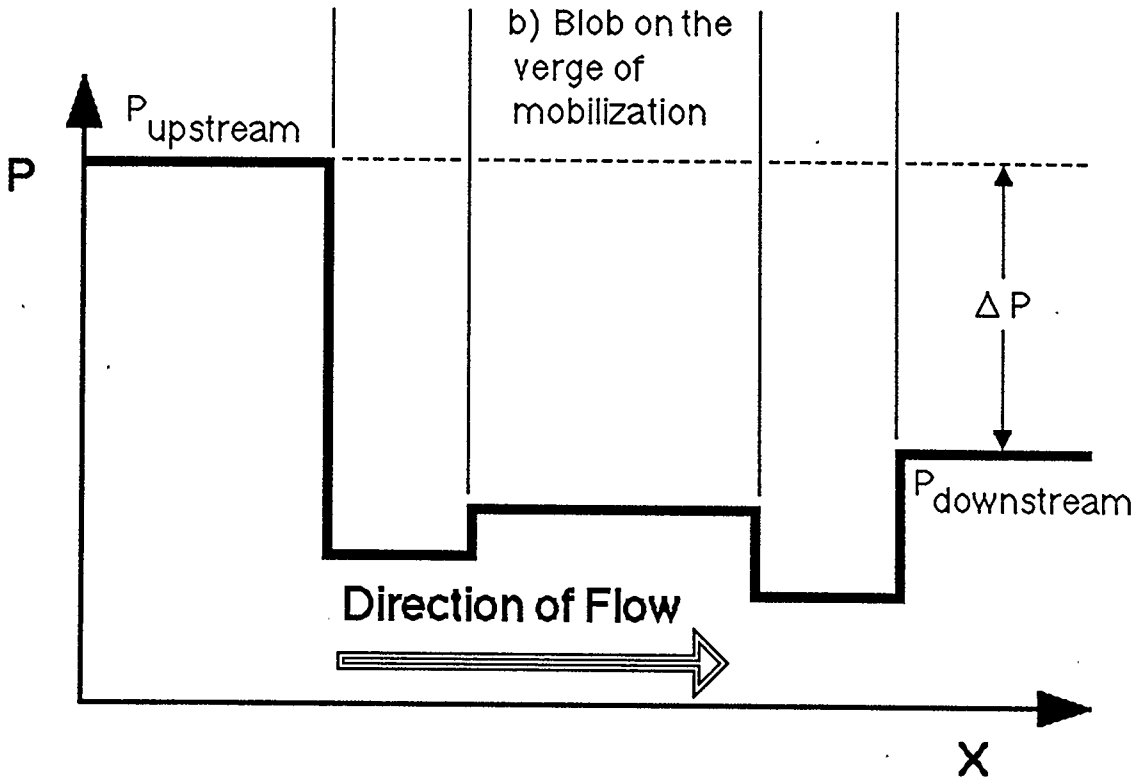

c) Schematic of pressure changes across water-oil and oil-gas interfaces, and mobilization pressure (ΔP)

Figure 4. The configuration of three phases (water, oil and gas) in a cylindrical capillary tube for oil-wet conditions.

respectively. When contact angle hysteresis and the radii of curvature are taken into consideration, the expression becomes :

$$\Delta P = 2\gamma [(\cos \theta_R / r_t) - (\cos \theta_A / r_p)] \qquad \text{(Eqn. 1.12a)}$$

or, alternatively :

$$\Delta P = [2\gamma / r_t] \ (\cos \theta_R - \{\cos \theta_A / \beta\}) \qquad \text{(Eqn. 1.12b)}$$

where $\beta = r_p / r_t$, or the pore to throat size ratio (aspect ratio).

The above equation reflects the maximum mobilization pressure for a blob of nonwetting phase with contact angle hysteresis in a converging-diverging pore system.

The mobilization of a blob of wetting phase (for example, oil in an oil-wetted rock) differs from that of a nonwetting phase because the wetting blob assumes a configuration which is different from that for the nonwetting blob. The leading edge of the wetting blob, where oil displaces water, is located at the widest part of the pore body; and the trailing edge of the blob, where water displaces oil, is located at the narrowest part of the throat. The expression for the mobilization of a blob of wetting phase is :

$$\Delta P = [2\gamma / r_t] \ (\{\cos \theta_R / \beta\} - \cos \theta_A) \qquad \text{(Eqn. 1.13)}$$

1.4 Effect of pore geometry on ganglia trapping and mobilization

The mobilization of trapped ganglia in a capillary of cylindrical shape is determined solely on the wetting characteristics of the solid surface, that is, the contact angle hysteresis of the two fluid-fluid interfaces. However, for capillaries which have a series of constrictions, the geometry of the medium has a more important influence on trapping and mobilization. Gardescu (1930) noted that the distortion of a gas bubble in a converging capillary tube under water-wet conditions required a much greater force than in a straight capillary

tube, primarily because of the change in the radius of curvature at the leading edge. Purcell (1950) and Stegemeier (1977) observed that trapping could occur in a pore-throat system under intermediate wetting conditions ($\theta = 90°$) depending on the position of the interface within the pore, since the interface is forced to bend whenever the pore wall is not normal to the axis of flow.

Using the toroidal pore model (Figure 5), Purcell (1950) defined a dimensionless quantity ($P_c\, r / 2\gamma$), which to related to the contact angle, the radius of curvature of the solid, the minimum radius of the pore and the position of the interface within the pore :

$$P_c\, r / 2\gamma = \cos(\theta - \alpha) / [1 + (R / r)(1 - \cos\alpha)] \qquad \text{(Eqn.1.14)}$$

where the maximum curvature exists at

$$\alpha_m = \theta - \arcsin[\sin\theta / \{1 + (r / R)\}] \quad \text{(Stegemeier, 1977)} \qquad \text{(Eqn. 1.15)}$$

and P_c = the capillary pressure across the interface
(i.e. the pressure difference between the two fluids)

γ = the interfacial tension between the fluids

θ = the contact angle

α = the position of the interface

R = the radius of curvature of the torus

r = the minimum radius of the pore

The ratio R / r for most rocks falls in the range from 3 to 10, while for shapes common in clean sandstones, R / r is 3 to 4 (Stegemeier, 1977).

The sign of the dimensionless quantity depends on the contact angle that the interface between the fluids (fluid 1 and fluid 2) makes with the solid surface. If the contact angle is measured in fluid 1 (denser phase) and the contact angle is less than 90°, when the interface is positioned at or near the minimum radius of the pore, the pressure in fluid 2 is greater than in fluid 1 (P_2

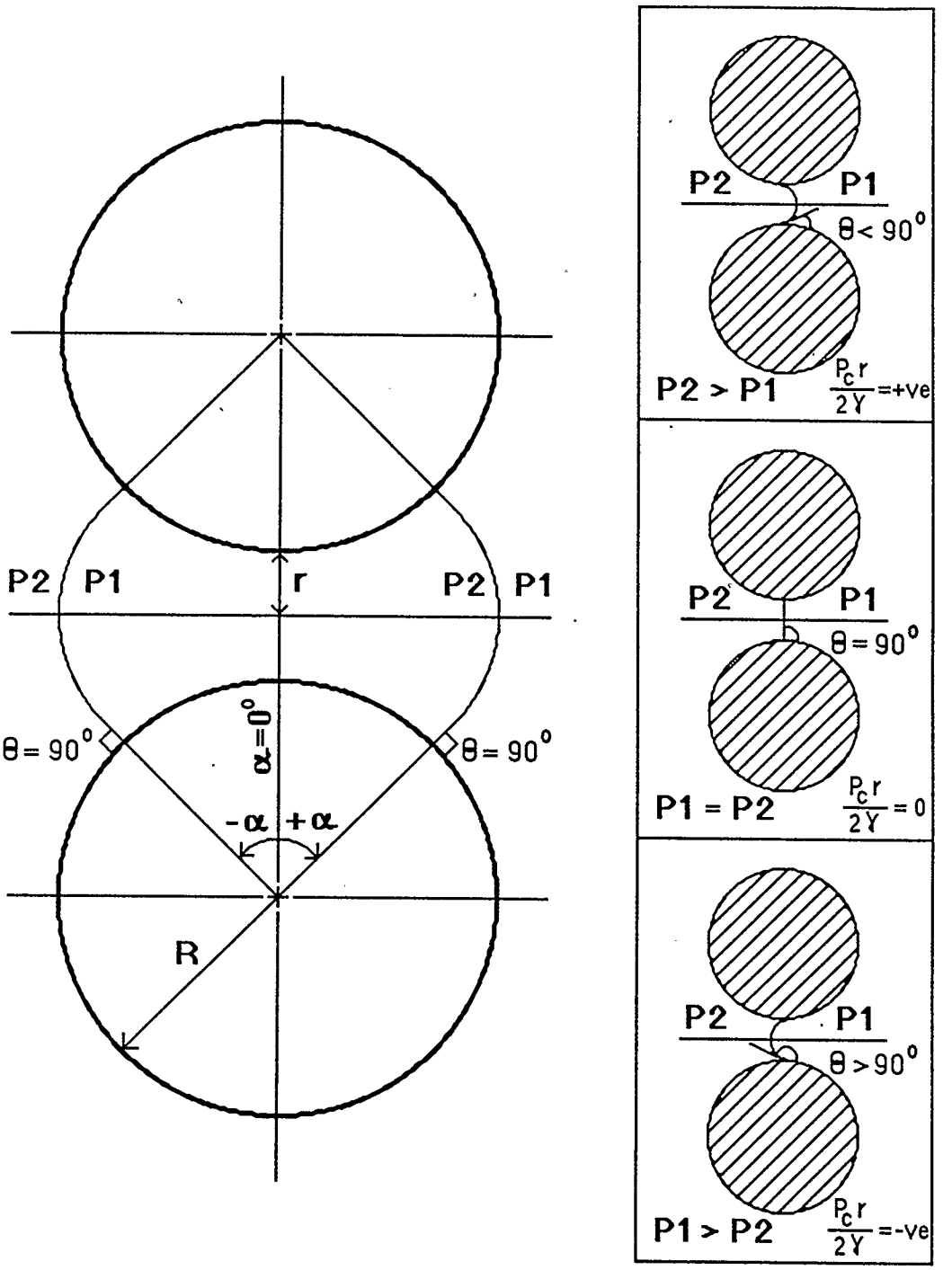

Figure 5. Configuration of a fluid-fluid interface in a toroidal pore model under different wetting conditions (after Purcell, 1950; and Stegemeier, 1977).

$> P_1$) and the dimensionless quantity is a positive value. Conversely, if the contact angle is greater than 90° at or near the minimum radius, the pressure in fluid 1 is greater than in fluid 2 ($P_1 > P_2$) and the dimensionless quantity is a negative value. For a contact angle equal to 90° at the minimum radius (α = 0°), there is no pressure difference across the interface ($P_1 = P_2$) and the dimensionless quantity is equal to zero. However, other than at the minimum radius (α = 0°), for intermediate wetting, the dimensionless quantity ($P_c r / 2 \gamma$) has a finite value and the interface is capable of sustaining a pressure.

Chapter 2 Materials and Fluid Properties

2.1 General Statement

This study of fluid mobilization is restricted to simple porous media of fixed geometry and known dimensions. Initial experiments were performed on capillary tubes of circular cross-section and constant diameter. These tubes were used as supplied by the manufacturer, except for the preparation of the two wettability conditions. The inner surfaces of the capillary tubes were not altered by additional roughening or smoothening. Morrow (1975) carried out experiments on smooth polytetrafluoroethylene (PTFE) tubes as supplied by the manufacturer, and classified the type of contact angle hysteresis observed as Class II behaviour. That is, the effect of contact angle on capillary rise is reasonably consistent from one tube to the next, and there is no overall systematic trend with respect to tube radius. It is expected that the tubes used in this current study will follow Class II type behaviour.

Later experiments were carried out in an etched glass micromodel. This model is comprised of a series of large pores which are circular in plan view and of approximately constant depth, and connected by narrower ducts of rectangular cross-section. The aspect ratio (i.e. pore to throat size ratio) is maintained at approximately 3; this ensures that the nonwetting phase will snap-off in the throats.

2.2 Fluid properties and methods of testing

The experiments were conducted under conditions of utmost cleanliness and purity of fluid phases in order to maintain repeatability and consistency of the experimental results. The fluids used in the experiments were air for "gas",

hexadecane for "oil" and distilled water for "brine". Hexadecane supplied from the manufacturer was doubly distilled through activated silica gel. Distilled water was obtained from a quartz distillation apparatus. It is necessary to obtain the fluid density of the three fluids and the interfacial tensions between the fluids.

Fluid density is measured with a PAAR Calculating Digital Density Meter. This is connected to a Lauda constant temperature bath, set at 22.5 °C. Table 2.1 gives the densities of hexadecane, distilled water and air.

The fluid density of distilled water in the PAAR instruction manual (from H. Wagenbreth and W. Blanke : "Die Dichte des Wassers im Internationalen Einheitensystem und in der Internationalen Praktischen Temperatureskala von1968") is given as 997.65 kg/m^3 at a temperature of 22.5 °C. The CRC Handbook of Chemistry and Physics (1986-1987 edition) gives the density of hexadecane as 773.3 kg/m^3 at 20.0 °C (p. C-301); and the density of air as 1.19 kg/m^3 at 23.0 °C (p. F-10). The measured values are : for water, 997.5 kg/m^3; for hexadecane, 771.6 kg/m^3; and for air, 1.1 kg/m^3, all at 22.5 °C.

Interfacial tension measurements are determined by the drop-weight (drop-volume) technique of Harkins and Brown (1919). A Gilmont digital micrometer syringe with a hypodermic needle of known radius is used to introduce drops of one fluid in the presence of the other fluid. The fluid breaks away from the needle tip forming spherical drops. For each liquid, the volume of one drop is obtained from the average of 10 drops formed successively. Interfacial tension is calculated from a set of correction factors, f(r/a), where r is the radius of the dropping tip, and a is the capillary constant, defined as (Wilkinson,1972) :

$$a = (2\gamma / \Delta\rho g)^{0.5} \qquad \text{(Eqn. 2.1)}$$

Table 2.1 Fluid Densities (kg/m^3) measured for hexadecane, distilled water and air (Temp. = 22.5 °C).

Measurement No.	Hexadecane	Distilled Water	Air
1	771.6	997.5	1.1
2	771.6	997.5	1.1
3	771.6	997.5	1.1
4	771.6	997.5	1.1
5	771.6	997.5	1.1
Avg	771.6	997.5	1.1

where γ = the interfacial tension between the two fluids

$\Delta\rho$ = the difference in density between the two fluids

g = the acceleration due to gravity (981 cm/s^2)

solving in terms of γ, the interfacial tension :

$$\gamma = (\Delta\rho\, g\, a^2) / 2 \qquad \text{(Eqn. 2.2)}$$

From Wilkinson (1972), the values of r/a for values of r/V between 0.060 and 1.049 are tabulated. The radius of the dropping tip used is .0451 cm. The surface tensions of hexadecane and water are given in Tables 2.2 and 2.3, respectively. The interfacial tension between hexadecane and water is given in Table 2.4.

The surface tension of water against air is given in the CRC Handbook of Physics and Chemistry as 72.75 mN/m at 20 °C (p. F-32). From Melrose (1964), in Contact Angle, Wettability, and Adhesion, edited by R.F. Gould, the surface tension of hexadecane against air is given as 27.6 mN/m. The interfacial tension of hexadecane against water is given by Wardlaw and Wright (unpublished report,1984) as 36.63 mN/m. This compares with the measured values of 71.37 mN/m for the surface tension of water; 27.41 mN/m for the surface tension of hexadecane; and 37.48 mN/m for the interfacial tension of hexadecane against water.

2.3 Design of glass micromodels

Transparent two-dimensional glass micromodels provide a means of observing fluid-fluid interactions in the confines of a porous medium of fixed topology. Wardlaw (1980 and 1982) and Wardlaw and McKellar (1981) have shown that glass micromodels are ideal when qualitative observations are to be made. Current experiments require accurate pressure measurement. The

Table 2.2 Surface tension measurement for hexadecane/air using the drop-volume (drop-weight) technique (Temp. = 23.1 °C).

Test	1	2	3	4	5	6	7
No. drops	10	10	10	10	10	10	10
Start (E-04 ml)	10632	13870	14649	16248	17049	19490	23599
Stop (E-04 ml)	9840	13073	13870	15415	16248	18665	22758
Difference	792	797	769	833	781	825	841
Volume per drop (ml)	.00792	.00797	.00769	.00833	.00781	.00825	.00841
r (cm)	.0451	.0451	.0451	.0451	.0451	.0451	.0451
$V^{1/3}$	.1993	.1997	.1974	.2027	.1984	.2021	.2034
$r/V^{1/3}$	.2263	.2258	.2285	.2225	.2273	.2232	.2218
r/a	.1688	.1682	.1711	.1649	.1698	.1656	.1641
a	.2672	.2681	.2636	.2735	.2656	.2723	.2748
γ	26.97	27.17	26.25	28.27	26.66	28.03	28.54

The average surface tension of hexadecane against air is 27.41 mN/m.

Table 2.3 Surface tension measurement for distilled water/air using the drop-volume (drop-weight) technique (Temp. = 23.1 °C).

Test	1	2	3	4	5	6
No. drops	10	10	10	10	10	10
Start (E-04 ml)	14878	16620	18345	20079	17080	20422
Stop (E-04 ml)	13203	14878	16620	18345	15400	18705
Difference	1675	1742	1725	1734	1680	1717
Volume per drop (ml)	.01675	.01742	.01725	.01734	.01680	.01717
r (cm)	.0451	.0451	.0451	.0451	.0451	.0451
$V^{1/3}$	.2559	.2592	.2584	.2588	.2561	.2580
$r/V^{1/3}$	.1763	.1740	.1745	.1742	.1761	.1748
r/a	.1193	.1171	.1175	.1173	.1191	.1178
a	.3781	.3851	.3837	.3845	.3787	.3828
γ	69.87	72.49	71.93	72.27	70.09	71.60

The average surface tension of distilled water against air is 71.37 mN/m.

Table 2.4 Interfacial tension measurement for hexadecane against distilled water using drop-volume (drop-weight) technique (Temp. = 23.1°C).

Test	1	2	3	4	5	6	7
No. drops	10	10	10	10	10	10	10
Start (E-04 ml)	24209	16239	20355	24426	14519	18584	22628
Stop (E-04 ml)	19564	11820	16239	20355	10454	14519	18584
Difference	4645	4419	4116	4071	4065	4065	4044
Volume per drop (ml)	.04645	.04419	.04116	.04071	.04065	.04065	.04044
r (cm)	.0451	.0451	.0451	.0451	.0451	.0451	.0451
$V^{1/3}$	.3595	.3535	.3453	.3440	.3438	.3438	.3432
$r/V^{1/3}$	.1255	.1276	.1306	.1311	.1312	.1312	.1314
r/a	.0740	.0757	.0783	.0787	.0788	.0788	.0790
a	.6096	.5955	.5761	.5731	.5725	.5725	.5712
γ	41.16	39.29	36.78	36.39	36.31	36.31	36.15

The average interfacial tension of hexadecane against distilled water is 37.48 mN/m.

glass micromodels, as used previously, were sealed because of material balance considerations but allowed fluid flow above the etched pattern in the so-called "pillar spaces". The surface heterogeneities of the model and cover plates result in a finite separation of approximately 15 microns between the plates (i.e. pillar space). Because fluid flow is not restricted to the etched pattern, mobilization pressures for the discontinuous phases are inaccurate. Therefore, it is necessary to bond the two plates together in a manner which preserves the high aspect ratio and visual nature of the model and permits the measurement of pressure along the prescribed flow path. This is accomplished by fusing the glass plates together in a high temperature oven.

The micromodel is designed with a simple pore-throat system having a moderate aspect ratio, at least greater than 2.5 to ensure nonwetting phase snap-off in the throats. A recent study by Li and Wardlaw (1986) indicated that snap-off occurs at an aspect ratio of 1.75 ($\theta \sim 55^{o}$), and that for contact angles greater than 70^{o}, no snap-off can occur. The aspect ratio of about 2.5 can be considered as being typical for a well sorted fine-grained sandstone of rhombohedral packing with porosity of approximately 26 percent (Berg, 1975).

Previous work (Wardlaw, 1986) with similarly produced glass micromodels indicated two basic problems involved with model fabrication. The first was a limit to the depth of etch that is achievable with the hydrofluoric acid, on the order of 170 to 180 microns. The second was with the undercutting of the protective silver and copper layers which define the etch pattern. This undercutting resulted in an overetch of about 80 microns in the width of the pattern regardless of the original dimension. Therefore, the size and aspect ratio of the pores and throats in the model had to be designed on the basis of the effective diameter of the elements in the model. The effective diameter is

the equivalent dimension for an irregular shaped pore which, by nature, is non circular. Lenormand et al (1983) defined effective diameter (d_e) for pathways of rectangular or elliptical cross-section, in which the dimensions of cross-section, width and height, or principal axes, are x and y, as :

$$d_e = \frac{2}{(1/x + 1/y)} \qquad \text{(Eqn. 2.3)}$$

This equation shows that d_e is dependent on the magnitudes of both the width of etch (x) and the depth of etch (y). If, for example, x were equal to y, then d_e would be the same magnitude as either x or y. If, however, x is significantly greater than y, as is the case with etched micromodels, then the variable which most affects the size of d_e would be the smaller of the two, namely, the depth of etch (y).

$$d_e = \frac{2}{(1/x + 1/y)}$$

$$d_e = \frac{2xy}{x + y} \qquad \text{(Eqn. 2.4)}$$

for $x >> y$, $d_e = 2y$

From previous micromodels, it was noted that the maximum depth of etch varied for pores and throats. Throats had a depth of etch of approximately 120 microns, and pores about 170 microns. Based on these dimensions, a pore-throat etch pattern with aspect ratio of about 2.8 to 2.9 is drafted. The only way this aspect ratio can be achieved with the limitation on depth of etch is to etch the pores and throats into the lower or model plate, and the pores only, into the upper or cover plate. The drafted pattern is larger than the desired image size by exactly four times to ensure the accuracy of the detail. The drawing is photographed and a photo positive black-and-white transparency, reduced by

four times, is produced for the etching process.

2.4 Fabrication of the glass micromodel

The method used in making glass micromodels is outlined by McKellar and Wardlaw (1982) and makes use of a photo imaging technique followed by chemical etching of the glass. Since the etching is accomplished with hydrofluoric acid, the photoresist layer from the photo imaging procedure cannot long withstand the acid attack by itself and requires an intermediate layer between the photoresist and the glass surface. Mirror, which is glass backed witha layer of silver, a layer copper and protective backing, is an ideal medium for making glass micromodels since both silver and copper are resistant to attack by hydrofluoric acid and yet are soluble in other acids such as dilute nitric acid. The procedure for making glass micromodels is outlined below :

A piece of mirror is cut to the appropriate size and placed in a hot (70 ^{o}C) solution of 200 gm of NaOH with sufficient distilled water to make 600 cc of solution. The protective backing slides off after approximately 10 minutes, exposing the copper layer, which is then washed with a jet of hot tap water. The mirror is examined in a darkened room under a microscope to check for an even copper-silver backing free of scratches and imperfections. In subdued light, undiluted Kodak KPR photoresist is applied to the copper backing and distributed evenly over the surface by tilting in several directions. The excess is drained off by holding the glass vertically on a paper towel. After 10 minutes, the glass is placed in an oven at 85 ^{o}C for 20 minutes and then allowed to cool.

A positive, black-and-white transparency of the desired model is now sandwiched against the resist coating with a piece of clean glass and exposed

to a 275 W sunlamp for approximately 10 minutes at a distance of 45 cm. The exact exposure time depends on photo resist thickness and the size of the pore elements in the model. Thicker resist requires longer exposure, but longer exposures affect fine detail adversely. The image is developed for not more than 3 minutes in Kodak KPR developer and normal room lighting is restored. The model is rinsed with tap water followed by distilled water to remove excess developer and developed resist, after which it is oven baked for 10 minutes at 120 °C and allowed to cool. The model is microscopically examined to ascertain the quality of the resist image and ensure that no unexposed resist remains on the copper.

The model is placed in a solution of 50 % nitric acid which removes the exposed copper and silver layers within 15 seconds, followed immediately by a distilled water rinse to halt the acid attack. The model is checked for a final time using transmitted light microscopy to determine whether the image is satisfactory for etching. Examination with reflected light may reveal a "milky" layer on the glass which will impair subsequent etching. This layer should be removed by immersion in a bath of sodium hydroxide followed by a forceful jet of hot tap water. A distilled water rinse is followed by further baking for 10 minutes at 120 °C.

Exposed portions of glass which are not to be etched are coated with paraffin wax and the model is placed face down in a 25 % solution of hydrofluoric acid for about 20 minutes. The model is rinsed in water, excess wax removed with benzene, excess resist removed with acetone and the remaining copper and silver removed with nitric acid, followed by a final rinse of hot water. The final result is ready for fusing.

2.5 Geometry of the micromodel

Prior to fusing the cover and model plates together, the dimensions of the different elements in the pattern must be determined. The measurement of the width of etch (x) of the pores and throats is achieved through the use of a Leitz optical microscope fitted with a graticule in one of the oculars. The depth of etch (y) is measured with the aid of the fine adjustment focussing knob, which measures the difference between the upper and lower focussed surfaces of the pore or throat etch pattern. The depth of focus is sufficiently narrow that the desired precision is possible. The microscope was calibrated for these measurements in the following manner :

i) The graticule in the 12.5X ocular has a fine scale of 200 graduation lines. This was used to measure an optical scale whose "coarse" divisions each represented 0.1 mm (i.e. 100 microns) thereby giving the number of graduation lines per 100 microns.

ii) "Feeler" gauges, thin flat pieces of metal of known thickness used by machinists in determining tolerances, were used to calibrate the fine focus knob by focussing on the metal surface with reflected light) and on the glass slide beneath the gauge (with transmitted light). The indicated gauge thickness was checked by using the already calibrated width measurement method. The gauges were placed on end and their thicknesses measured with the graticule scale. The calibration for three different objective lenses are presented in Table 2.5.

The pattern of the micromodel is arranged in the following manner : an inlet moat is connected to a linear series of 10 pores and then to an outlet moat by 11 throats of rectangular cross-section. The interconnecting throats all have a length of approximately 2.4 mm. The elements in the lower or model plate

Table 2.5 Calibration of the Leitz optical microscope for width and depth of etch measurement.

Objective Lens	Width (graticule) (number of divisions	Depth (fine focus knob) equivalent to 100 μm)
Leitz Wetzlar NPL Fluotar 2.5/0.08P	4.45	N.A.
Leitz Wetzlar NPL Fluotar 6.3/0.20 P	11.5	114
Leitz Wetzlar NPL Fluotar 16/0.45 P	29.0	110

are labelled : one of the moats is arbitrarily chosen to be the inlet moat I/L; the other being the outlet or O/L. The pores are labelled starting from the inlet I/L, PL/1, PL/2 and so on to PL/10. The throat between I/L and PL/1 is labelled TL/1, and so on to TL/11. The upper or cover plate is labelled in a like manner, except that there are no throats etched in the cover plates because of the necessity of enhancing the aspect ratio. Therefore, the moats are I/U and O/U. The pores are from PU/1 to PU/10. The dimensions of width and depth of etch are given for the elements in the lower plate in Table 2.6; for the upper plate, in Table 2.7. As well, the aspect ratios for the different pore-to-throat combinations in the model are given in Table 2.8.

The effective diameters of the individual pores and throats are calculated from Eqn. 2.3. The average effective diameter of the pores is 655.5 microns; the average effective diameter of the throats is 222.4 microns; and the average aspect ratio is 2.95. In shape, the pores are essentially pancake like pill boxes, while the throats are rectangular ducts (Figure 6). Since the throats are only etched in the model plate, the junction of throat and pore is a sharp edged orifice which may be of some consequence during mobilization. Once all measurements have been completed, 3.17 mm (1/8 inch) inlet and outlet ports are drilled into the inlet and outlet moats. The model and cover plates are aligned such that the upper and lower moats and pores match their labelled counterparts, and are epoxied together at three or four points along the edges of the plates. The model is placed on a flat smooth ceramic block in a high temperature oven.

The temperature is incrementally increased over 3 hours until 700 ^{o}C is reached. The model is allowed to remain at the temperature for 30 to 45 minutes, and then the temperature is incrementally reduced over another 3

Table 2.6 The width (x) and depth of etch (y) of the different elements in the lower (model) plate of the glass micromodel.

Type of Element (Moat, Pore or Throat)	Width of Etch (x)		Depth of Etch (y)	
	divisions	microns	divisions	microns
Moats				
I/L	189	4247	192	168
O/L	188	4225	196	172
	Avg	4236		170
Pores				
PL/1	186	4180	205	180
PL/2	184	4135	197	173
PL/3	186	4180	201	176
PL/4	187	4202	192	168
PL/5	186	4180	199	175
PL/6	187	4202	208	182
PL/7	188	4225	190	167
PL/8	188	4225	187	164
PL/9	185	4157	198	174
PL/10	186	4180	191	168
	Avg	4186		172
Throats				
TL/1	122	421	142	129
TL/2	126	434	152	138
TL/3	119	410	145	132
TL/4	127	438	154	140
TL/5	122	421	140	127
TL/6	121	417	143	130
TL/7	126	434	157	143
TL/8	131	452	149	135
TL/9	126	434	154	140
TL/10	125	431	152	138
TL/11	128	441	146	133
	Avg	430		135

Note : The widths of the pores and moats were measured with the Leitz Wetzlar 2.5/0.08 P objective lens. The widths of the throats and all the depths of etch were measured with the Leitz Wetzlar 16/0.45 P objective lens.

Table 2.7 The width (x) and depth of etch (y) of the different elements in the upper (cover) plate of the glass micromodel.

Type of Element (Moat or Pore)	Width of Etch (x) divisions	microns	Depth of Etch (y) divisions	microns
Moats				
I/U	187	4202	190	167
O/U	187	4202	200	175
	Avg	4202		171
Pores				
PU/1	188	4225	194	170
PU/2	187	4202	198	174
PU/3	189	4247	198	174
PU/4	188	4225	186	163
PU/5	188	4225	196	172
PU/6	188	4225	187	164
PU/7	186	4180	187	164
PU/8	187	4202	183	161
PU/9	187	4202	186	163
PU/10	187	4202	199	175
	Avg	4214		168

Note : The widths of the pores and moats were measured with the Leitz Wetzlar 2.5/0.08 P objective lens. The depths of the pores and moats were measured with the Leitz Wetzlar 16/0.45 P objective lens.

Table 2.8 The effective diameters (in microns) of the combined upper and lower pores, and the throats; and the aspect (pore-to-throat size) ratios.

Throat	Effective Diameter (D_t)	Aspect Ratio (D_p/D_t)	Pore	Effective Diameter (D_p)
TL/1	214.6			
		3.13	P 1	671.6
		2.97		
TL/2	226.5			
		2.94	P 2	665.3
		3.08		
TL/3	216.2			
		3.10	P 3	671.8
		2.93		
TL/4	228.9			
		2.80	P 4	640.5
		3.01		
TL/5	212.6			
		3.13	P 5	665.7
		3.09		
TL/6	215.2			
		3.09	P 6	665.8
		2.88		
TL/7	231.4			
		2.76	P 7	638.8
		2.83		
TL/8	225.7			
		2.78	P 8	628.4
		2.75		
TL/9	228.5			
		2.84	P 9	649.0
		2.87		
TL/10	226.0			
		2.91	P 10	658.1
		2.97		
TL/11	221.3			

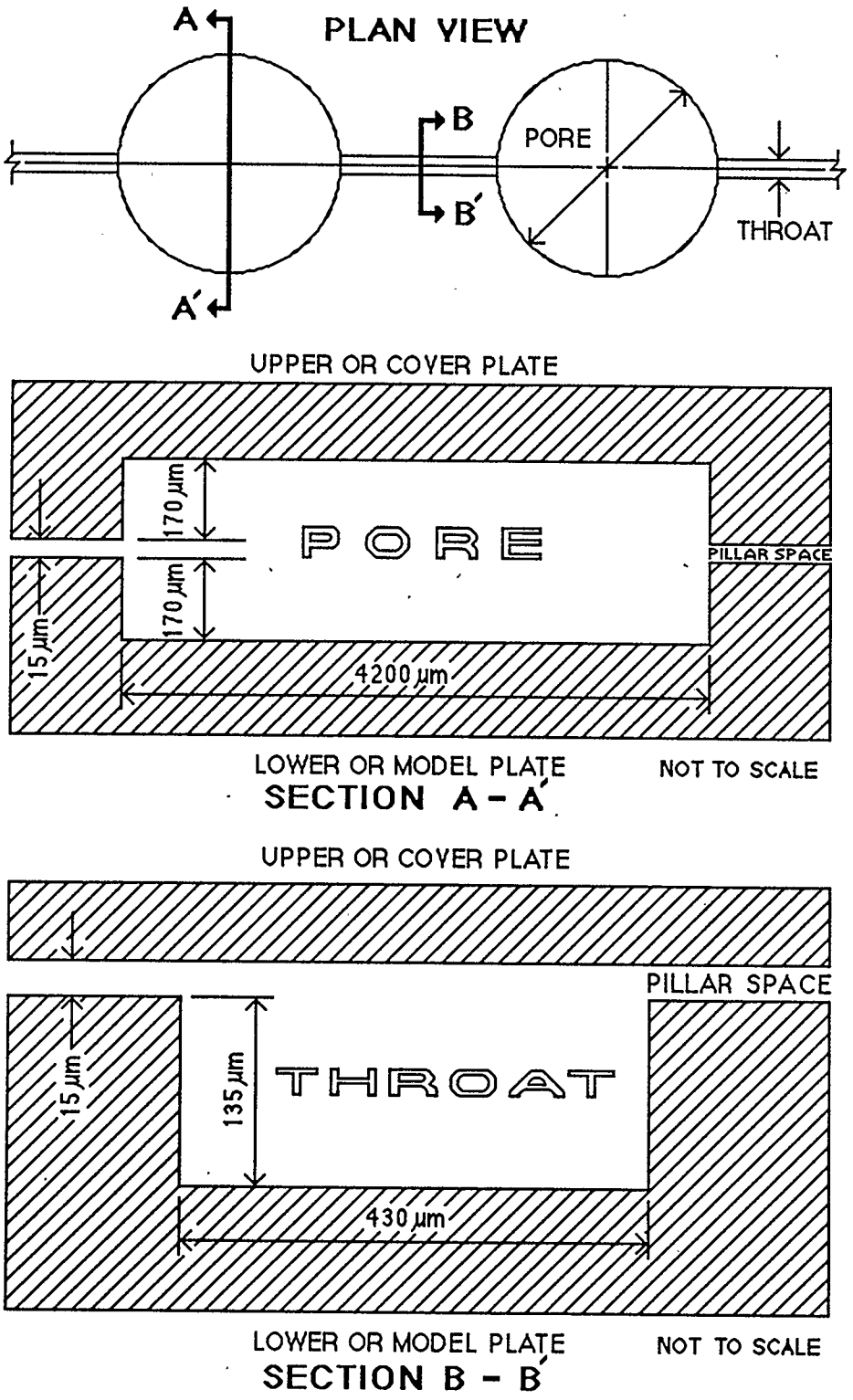

Figure 6. Cross section of pore and throat from glass micromodel.

hours, and the oven is turned off. At the end of this time, the oven temperature is still at about 450 °C, therefore the model remains in the oven overnight to cool. The model is checked with the microscope to ensure that the pillar spaces around the etch pattern are fused together.

Chapter 3 Capillary Tube Experiments

3.1 Description of Apparatus

The capillary tube experiments determine the effect of wettability on mobilization pressure in a cylindrical tube. The capillary tube used is a disposable 50 microliter pipet made of borosilicate glass. The inside diameter is 861 microns and was measured with a Leitz binocular microscope fitted with 25 and 50 power lenses which were calibrated for width measurement. The diameter of the tube was measured at various points along its length by simply breaking the tube at those locations. The tubes are essentially a "one-use" piece of apparatus because of contamination acquired during experimentation and the easily sustained breakage.

The capillary tubes were prepared for water wetting behaviour in the following manner : 1) a preliminary wash with liquid detergent and distilled water using a glass syringe and fine hypodermic needle; 2) a flush distilled water; 3) immersion in a warm 1 M NaOH solution for one to two days; and 4) a final flush with distilled water. Water-wet tubes were used immediately after the final flush to prevent contamination from air-borne dust, etcetera.

Oil-wet capillary tubes were prepared by : 1) the preliminary wash with liquid detergent and distilled water; 2) allowed to dry by draining and blotting with paper towels; 3) half filled with Surfasil, a siliconizing agent, and tilted back and forth for approximately 15 minutes; and 4) drained and blotted dry, and allowed to dry overnight in a dust free environment.

The apparatus designed to "capture" a bubble of the displaced phase, whether it be air, hexadecane, or hexadecane in combination with air, utilized a system of polypropylene tubing, valves and syringes. This caused

contamination when experiments were carried out on water-wet tubes. The original water-wet condition was rendered oil-wet in a very short period of time. As the method was still viable, the polypropylene materials which caused contamination in the sensitive areas of the experiment apparatus were replaced by glass and steel fittings. Thereafter, the glass and steel fittings were thoroughly disassembled and cleaned of all contaminants with the use of solvents, flushed with distilled water and soaked in NaOH solution, at the termination of each experiment.

The capillary tube is attached to a glass T-joint by a metal sleeve and epoxy cement. The T-joint is, in turn, attached to a three way steel stopcock, which seals the apparatus once a bubble has been placed in the capillary tube. Hexadecane is introduced with a glass Multifit syringe with a two way steel stopcock; and air, by a precision volume syringe with screw adjustable plunger (Figure 7). Bubbles of either or both phases are injected into the glass T-joint. At the junction of the T, the different phases are manipulated until an appropriate sized bubble is attained. The bubble size is restricted by the frame size of the photographic image. In order to get an image of all fluid-fluid interfaces, the maximum bubble length is approximately 5 millimeters. The capillary tube is fixed into a jig which is attached to the front of the camera bellows focussing rail, this rail is placed on a tilting three way head tripod stand.

Preliminary experiments indicated that mobilization pressures for water-wet conditions were appreciably less than for equivalent oil-wet conditions. Therefore, individual methods of pressure measurement were devised for the water-wet and oil-wet conditions.

The measurement of pressure for water-wet experiments was accomplished by the tilting of the capillary tube with the tripod head and

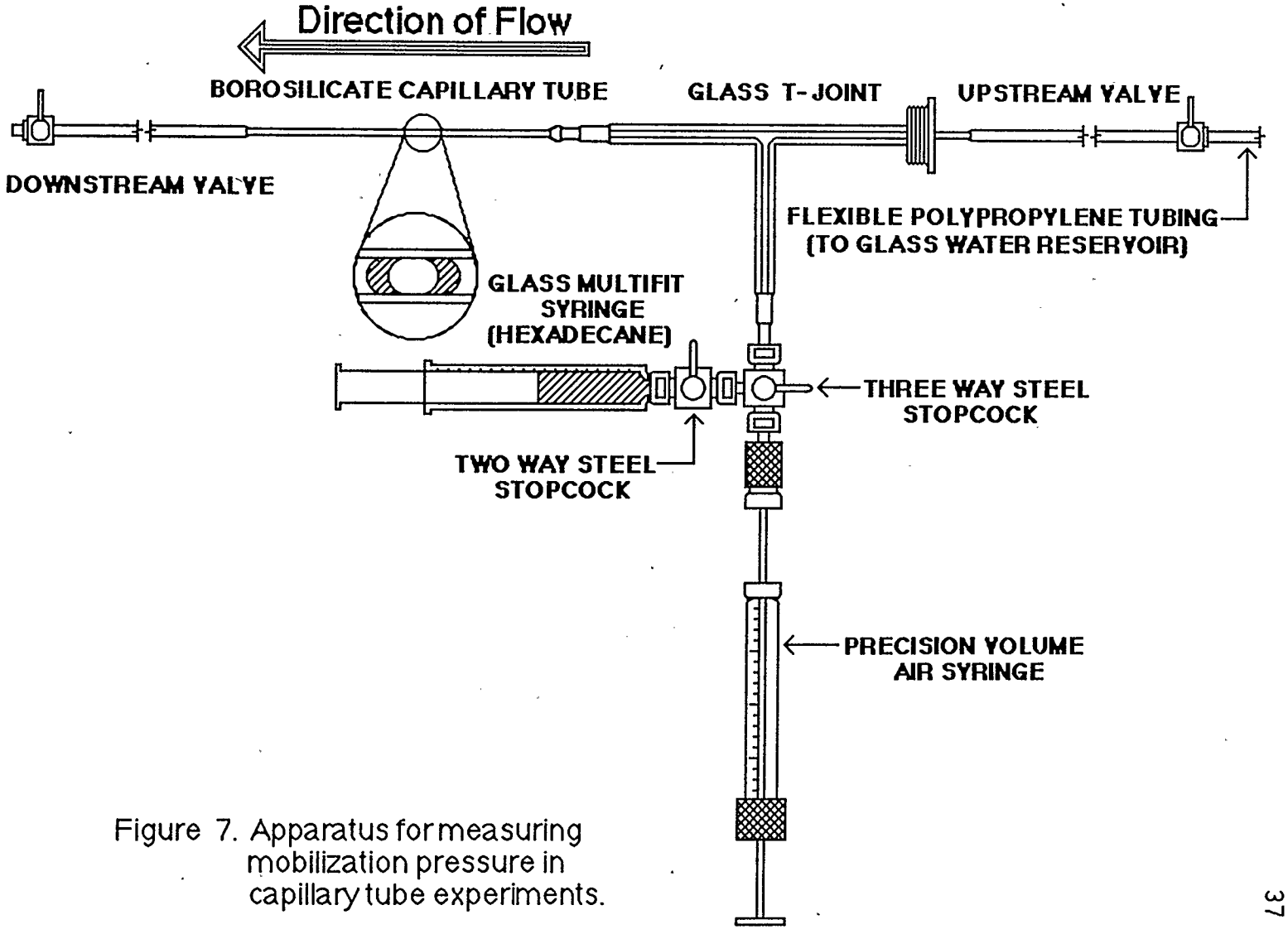

Figure 7. Apparatus for measuring mobilization pressure in capillary tube experiments.

recording the critical angle at which the oil or gas bubble just begins to move up the tube. A goniometer scale is affixed to the rear of the bellows focussing rail. When the tube is horizontal, the goniometer reads zero angle from a weighted plumb bob. As the tripod head is tilted, the plumb bob indicates the angle of tilt on the goniometer scale. The camera is also being tilted, so the photographs do not indicate any angle of tilt. The camera is used to record the advancing and receding contact angles at the interfaces.

The measurement of pressure for oil-wet experiments uses a water reservoir attached to the upstream end of the bubble. Pressure is applied by the addition of water to this reservoir by a calibrated buret. The head difference is easily calculated from the volume of water added and the measured diameter of the circular reservoir.

3.2 Experimental Procedure

The "capture" of a bubble is the same for both water-wet and oil-wet tubes. The capillary tube and attached apparatus are placed on a horizontal stage with the upstream water reservoir slightly elevated. The three way stopcock connecting the T-joint to the hexadecane and air syringes is closed. Deaerated distilled water is flowed through the flexible tubing, glass T-joint and capillary tube. This is accompanied by mild to vigorous shaking of the apparatus to remove the trapped air in the system.

Depending on which phases are to be mobilized, hexadecane and/or air are introduced into the junction of the T-joint. Because the junction has a greater volume than the connecting arms of the T-joint, a small spherical bubble in the junction becomes a long cylindrical bubble in the exit arm as well as in the capillary tube. At this point, careful manipulation of the apparatus is

necessary to attain a bubble which will be less than 5 millimeters within the capillary tube. Once a bubble is obtained, it is carried into the capillary tube by a combination of water flow from the reservoir and air from the air syringe. Care should be taken that, when the three way stopcock is closed, the only interfaces in the system are those of the bubble. The upstream and downstream valves are then closed effectively immobilizing the bubble.

For water-wet experiments, the extraneous attachments such as the water reservoir, the hexadecane and air syringes are removed, and the capillary tube, glass T-joint and flexible tubing are fixed in the camera attachment. The upstream and downstream ends of the flexible tubing are positioned at the same elevation above the tube and the end valves are carefully opened. The bubble is now in a state of static equilibrium, with only buoyancy and capillary forces acting on it. The tripod head is tilted to cause an increase in buoyancy force. Imminent bubble movement is preceded by a consistent vibration of the fluid-fluid interfaces. The position of imminent mobilization is recorded by its critical angle of tilt and a photograph is taken to record the advancing and receding contact angles.

In the oil-wet experiments, the water reservoir is retained along with the other apparatus. This is positioned on the bellows focussing rail as with the water-wet case. The downstream end of the flexible tubing is placed at the same elevation as the water level in the reservoir and the end valves are opened. Water from the buret is added to the reservoir. As sufficient pressure builds in the upstream end of the tube, the bubble shows increased distortion of its interfaces until it is eventually mobilized. This is recorded by the volume of water added to the reservoir and the photograph of the advancing and receding contact angles.

3.3 Experimental Data

Mobilization pressure is determined by two independent means for the water-wet and oil-wet experiments and the results compared. For water-wet experiments, the pressure acting on the bubble due to buoyancy can be calculated from the critical angle of tilt associated with imminent movement and the length of the different phases that comprise the bubble. These lengths are measured from the photographs. The equation for the buoyant pressure on a combined hexadecane-air bubble is (Refer to Figure 8) :

$$\Delta P = g \sin \alpha_c [\rho_w (L_o + L_g) - \rho_o L_o - \rho_g L_g] \qquad \text{(Eqn. 3.1)}$$

where α_c = the critical angle of tilt

g = the acceleration due to gravity

ρ = the density of the different phases

L_o = the length of the hexadecane portion of the bubble

L_g = the length of the air portion of the bubble

The subscripts o, w and g refer to oil, water and gas, respectively.

The above equation can be reduced to give the buoyant pressure for a bubble of hexadecane by itself and air by itself. For a bubble of hexadecane, the modified equation is :

$$P = L_o \; g \; \sin \alpha_c (\rho_w - \rho_o) \qquad \text{(Eqn. 3.2)}$$

For a bubble of air, the equation is :

$$P = L_g \; g \; \sin \alpha_c (\rho_w - \rho_g) \qquad \text{(Eqn. 3.3)}$$

Tables 3.1, 3.3 and 3.5 give the critical angle of tilt, L_o and/or L_g, and mobilization pressure for experiments where the displaced phases are air, hexadecane and hexadecane/air, respectively, and the displacing phase is water.

The second means by which mobilization pressures for water-wet

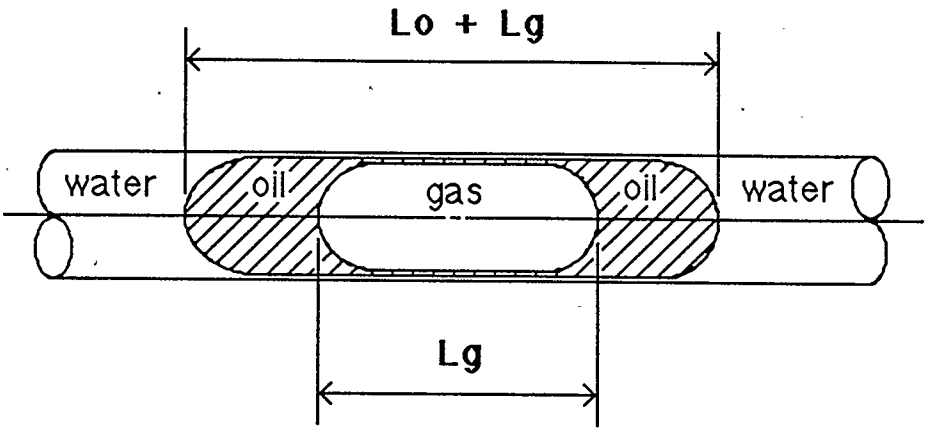

Lo is the length of the hexadecane portion of the bubble
Lg is the length of the air portion of the bubble

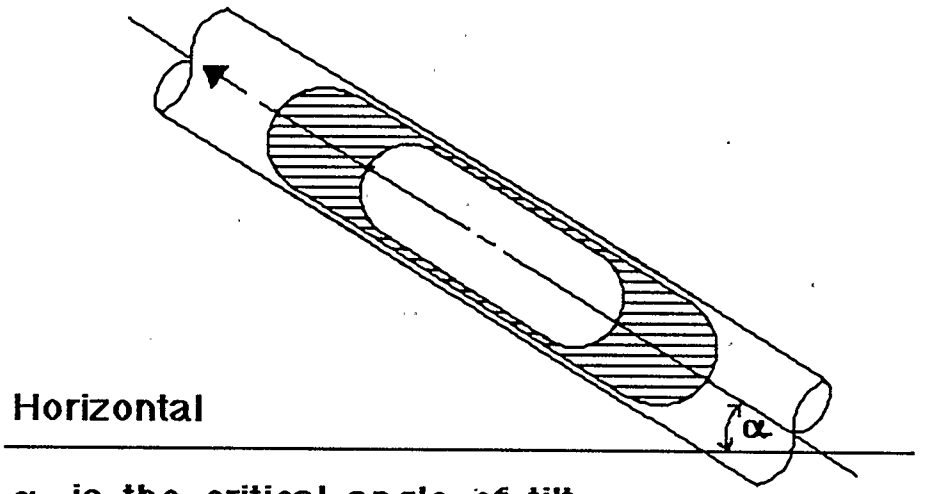

α_c is the critical angle of tilt

Figure 8. Buoyant pressure acting on an oil-gas bubble in a capillary tube with water-wet conditions. The critical angle of tilt indicates the imminent movement of the bubble up the tube.

Table 3.1 Mobilization pressures for air in a water-wet capillary tube, obtained from the critical angle of tilt and the length of the bubble.

Length of Air L_g (mm)	Critical Angle (degrees)	Pressure (Pa)
3.1	4.0	2.11
3.0	3.5	1.85
3.1	3.5	1.86
3.1	3.0	1.58
3.0	4.0	2.09
3.1	3.0	1.58
		Avg 1.85

Table 3.2 Mobilization pressures for air in a water-wet capillary tube, obtained from contact angle measurements.

Advancing Contact Angle θ_{Awo} (degrees)	Receding Contact Angle θ_{Row} (degrees)	Pressure (Pa)
6.0	3.8	1.07
6.0	3.8	1.07
7.5	3.8	2.07
6.7	4.6	1.24
5.3	3.1	0.90
9.0	7.5	1.25
Avg 6.7	4.4	1.27

Table 3.3 Mobilization pressures for hexadecane in a water-wet capillary tube, obtained from the critical angle of tilt and the length of the bubble.

Length of Hexadecane (mm)	Critical Angle (degrees)	Pressure (Pa)
4.0	42.5	6.03
4.0	40.0	5.74
4.0	46.0	6.42
4.0	41.5	5.92
4.0	46.0	6.42
4.3	39.0	6.00
5.0	32.0	5.87
4.0	49.0	6.77
4.0	53.0	7.17
4.0	52.0	7.07
4.0	56.0	7.44
4.0	53.0	7.17
4.0	54.0	7.26
		Avg 6.56

Table 3.4 Mobilization pressures for hexadecane in a water-wet capillary tube, obtained from contact angle measurements.

Advancing Contact Angle θ_{Awo}(degrees)	Receding Contact Angle θ_{Row}(degrees)	Pressure (Pa)
16.2	6.0	5.99
12.1	5.3	3.14
12.9	3.8	4.02
16.2	7.5	5.46
14.6	3.8	5.08
15.4	4.6	5.56
16.2	6.0	5.85
15.9	6.8	5.31
15.1	3.4	5.52
15.9	4.4	5.98
Avg 15.1	5.2	5.19

Table 3.5 Mobilization pressures for hexadecane/air in a water-wet capillary tube, obtained from the critical angle of tilt and the lengths of the two phases.

Length of Hexadecane L_o (mm)	Length of Air L_g (mm)	Critical Angle (degrees)	Pressure (Pa)
0.6	2.8	16.0	7.94
0.6	2.8	18.0	8.89
0.6	2.8	14.0	6.96
0.6	2.8	16.0	7.94
0.6	2.8	17.0	8.42
0.6	2.8	18.0	8.89
0.7	2.8	18.0	8.94
0.7	2.8	17.0	8.46
0.7	2.8	16.0	7.97
0.7	2.8	18.0	8.94
0.7	2.8	19.0	9.42
0.7	2.8	17.0	8.46
			Avg 8.44

Table 3.6 Mobilization pressures for hexadecane/air in water-wet capillary tube, obtained from contact angle measurements.

Contact Angles for Hexadecane/Water (degrees)		Contact Angles for Hexadecane/Air (degrees)		Pressure (Pa)
θ_{Awo}	θ_{Row}	θ_{Aog}	θ_{Rgo}	
17.0	6.8	19.2	18.1	7.16
15.9	6.3	22.7	20.9	7.04
15.3	5.4	22.1	19.8	7.27
15.3	6.3	21.5	20.3	6.07
16.4	6.8	18.6	17.5	6.66
14.4	5.1	23.2	22.1	5.75
15.3	6.8	21.5	19.8	6.34
15.9	6.3	20.9	18.6	7.30
15.7	6.2	21.2	19.6	Avg 6.70

experiments can be determined is from the photographs taken at imminent mobilization (Plates 1 A, 2 A and 3 A). The various fluid-fluid interfaces assume maximum advancing and receding contact angles just prior to bubble mobilization. Contact angles are calculated based on the inside diameter of the capillary tube and the height of the meniscus rather than by direct measurement of the photograph. This is necessary because the curvature of the tube causes enough distortion to make direct measurements invalid. A complete explanation of contact angle determination is included in Appendix A.2. Mobilization pressures are calculated by substituting advancing and receding contact angles into Eqn. 1.10. Tables 3.2, 3.4 and 3.6 give the advancing and receding contact angles and the mobilization pressures for air, hexadecane and hexadecane/air systems, respectively, where water is the displacing phase.

For oil-wet experiments, the mobilization pressures are determined from the calculated surface area of the water reservoir and the measured volume of water added by the buret. The water reservoir is of circular cross-section with a diameter of 7.30 centimetres. From the geometry of simple solids (a cylinder) :

$$V = \pi r^2 h \qquad \text{(Eqn. 3.4)}$$

where V = the volume of water added by the buret

r = the radius of the water reservoir

h = the change in level of water in the reservoir

(head of water required to mobilize bubble)

The mobilization pressure can be calculated from :

$$P = \rho g h \qquad \text{(Eqn. 3.5)}$$

where ρ = the density of water

g = the acceleration due to gravity

h = head of water required to mobilize bubble

Plate 1

A Water-wet capillary tube, displaced phase is air, displacing phase is water. The direction of flow is indicated by the arrow. Upper photograph shows static bubble with no externally applied pressure gradient. Lower photograph shows bubble on the verge of mobilization, with maximum advancing and receding contact angles. Mobilization pressure from contact angle hysteresis is 1.24 Pa.

B Oil-wet capillary tube, displaced phase is air, displacing phase is water. The direction of flow is indicated by the arrow. Upper photograph shows static bubble with no externally applied pressure gradient. Lower photograph shows bubble on the verge of mobilization, with maximum advancing and receding contact angles. Mobilization pressure from contact angle hysteresis is 44.7 Pa.

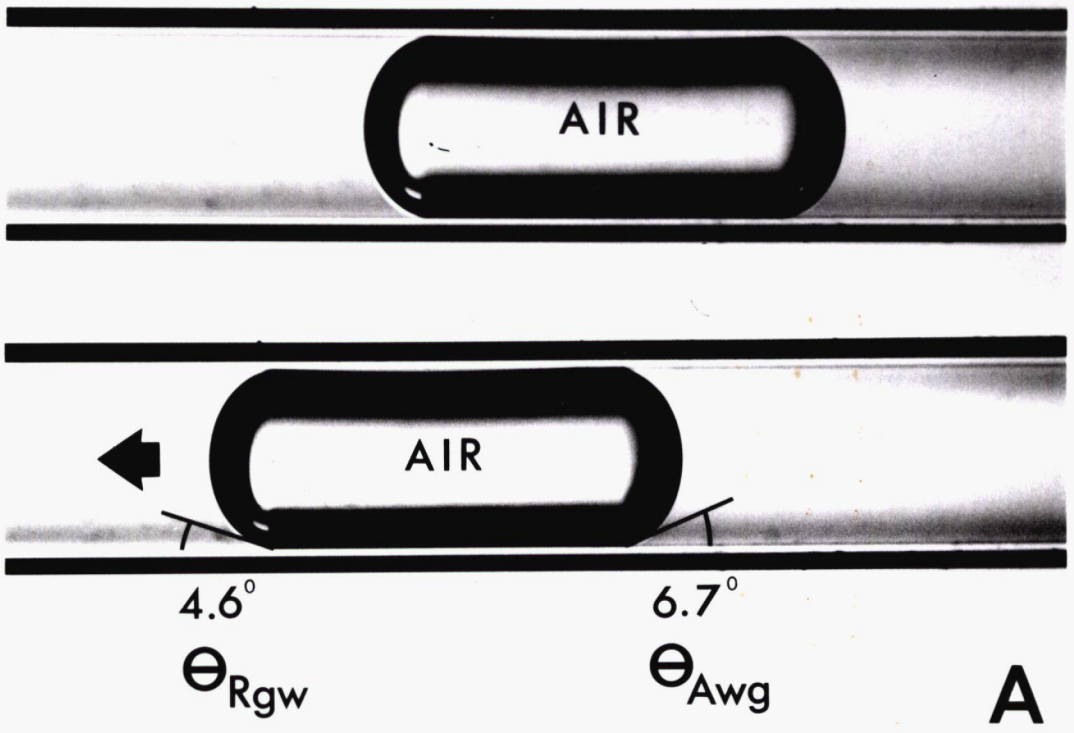
AIR
AIR
4.6°
6.7°
Θ_{Rgw}
Θ_{Awg}
A

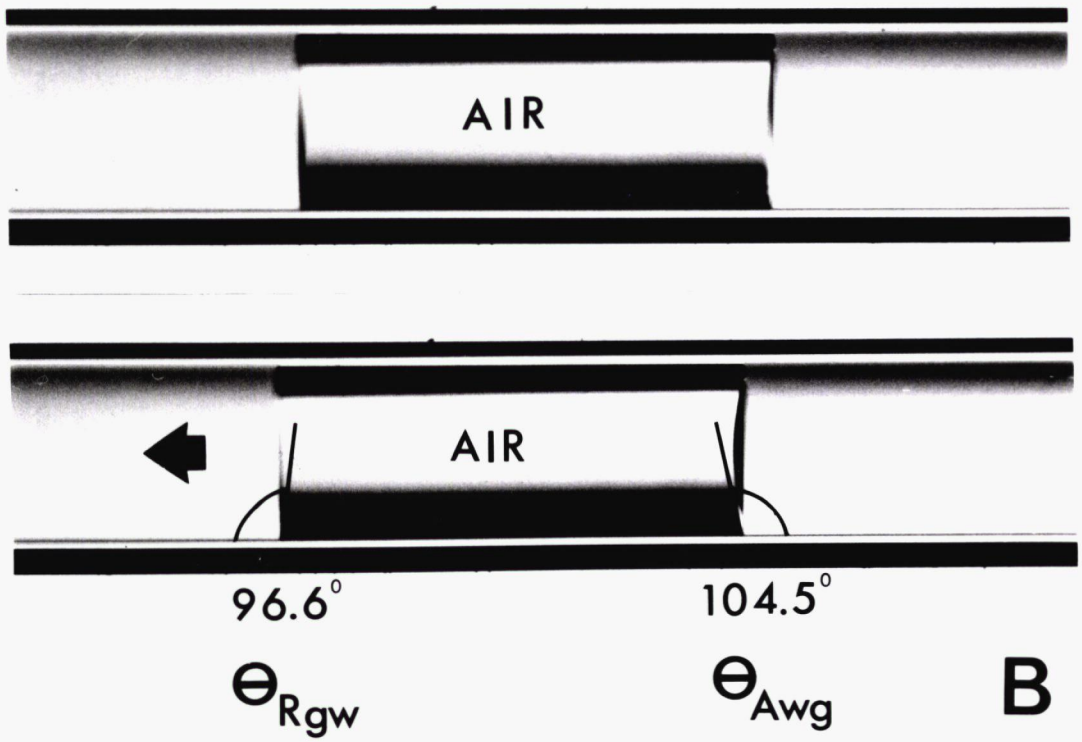
AIR
AIR
96.6°
104.5°
Θ_{Rgw}
Θ_{Awg}
B

Plate 2

A Water-wet capillary tube, displaced phase is hexadecane, displacing phase is water. The direction of flow is indicated by the arrow. Upper photograph shows static bubble with no externally applied pressure gradient. Lower photograph shows bubble on the verge of mobilization, with maximum advancing and receding contact angles. Mobilization pressure from contact angle hysteresis is 5.31 Pa.

B Oil-wet capillary tube, displaced phase is hexadecane, displacing phase is water. The direction of flow is indicated by the arrow. Upper photograph shows static bubble with no externally applied pressure gradient. Lower photograph shows bubble on the verge of mobilization, with maximum advancing and receding contact angles. Mobilization pressure from contact angle hysteresis is 59.1 Pa.

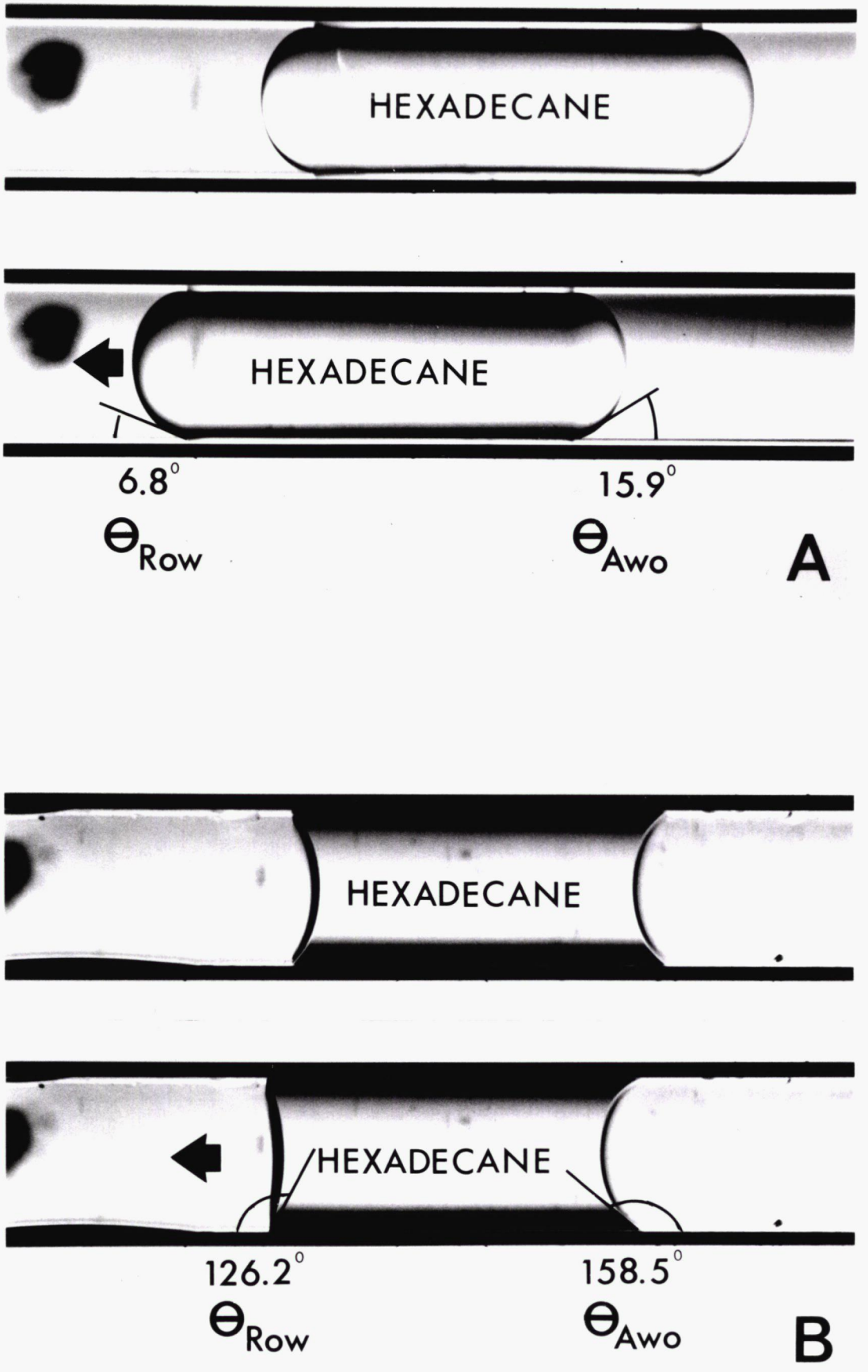
HEXADECANE
HEXADECANE
6.8°
15.9°
Θ_{Row}
Θ_{Awo}
A
HEXADECANE
HEXADECANE
126.2°
158.5°
Θ_{Row}
Θ_{Awo}
B

Plate 3

A Water-wet capillary tube, displaced phase is hexadecane/air, displacing phase is water (**H** is Hexadecane). The direction of flow is indicated by the arrow. Upper photograph shows static bubble with no externally applied pressure gradient. Lower photograph shows bubble on the verge of mobilization, with maximum advancing and receding contact angles. Mobilization pressure from contact angle hysteresis is 7.04 Pa.

B Oil-wet capillary tube, displaced phase is hexadecane/air, displacing phase is water (**H** is Hexadecane). The direction of flow is indicated by the arrow. Upper photograph shows static bubble with no externally applied pressure gradient. Lower photograph shows bubble on the verge of mobilization, with maximum advancing and receding contact angles. Mobilization pressure from contact angle hysteresis is 68.8 Pa.

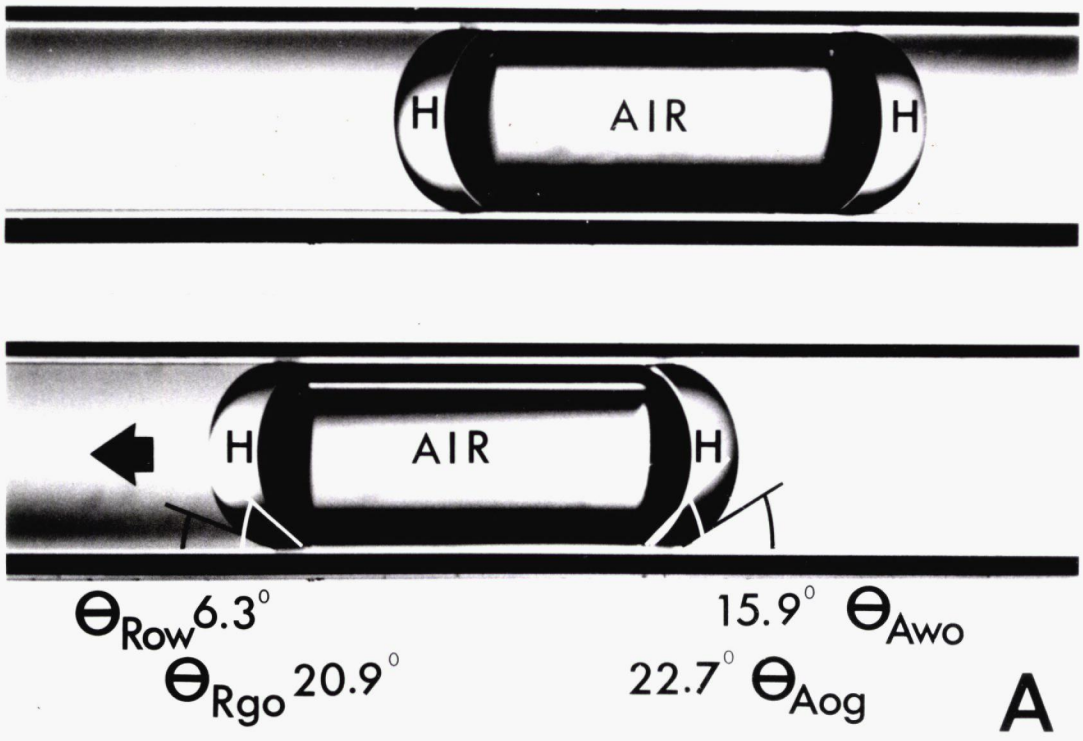
H
AIR
H
H
AIR
H
Θ_{Row} 6.3°
Θ_{Rgo} 20.9°
15.9° Θ_{Awo}
22.7° Θ_{Aog}
A

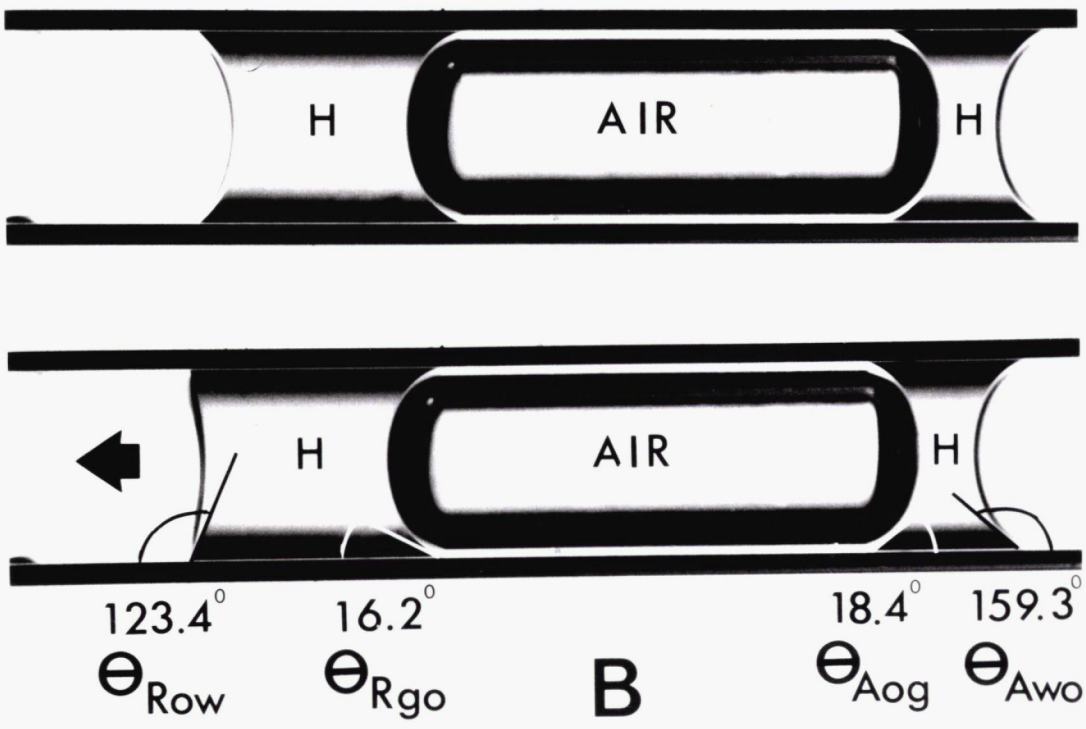
H
AIR
H
H
AIR
H
123.4°
Θ_{Row}
16.2°
Θ_{Rgo}
B
18.4°
Θ_{Aog}
159.3°
Θ_{Awo}

Tables 3.7, 3.9 and 3.11 give the volume, head and mobilization pressure for experiments where the displaced phases are air, hexadecane and hexadecane/air, respectively, and the displacing phase is water. The second method of determining pressure uses the advancing and receding contact angles calculate from the photographs, by the same method as in water-wet experiments, and Eqn. 1.11 (Plates 1 B, 2 B and 3 B). Tables 3.8, 3.10 and 3.12 give the advancing and receding contact angles and mobilization pressures for air, hexadecane and hexadecane/air systems, respectively, where water is the displacing phase.

Table 3.7 Mobilization pressures for air in an oil-wet capillary tube, obtained from buret volume and head of water in reservoir.

Volume (ml)	Head of Water (mm)	Pressure (Pa)
16.8	4.01	39.3
17.2	4.11	40.2
17.0	4.06	39.7
17.4	4.16	40.7
17.3	4.13	40.4
17.1	4.08	40.0
17.5	4.18	40.9
17.3	4.13	40.4
	Avg	40.2

Table 3.8 Mobilization pressures for air in an oil-wet capillary tube, obtained from contact angle measurements.

Advancing Contact Angle θ_{Awo} (degrees)	Receding Contact Angle θ_{Row} (degrees)	Pressure (Pa)
105.8	97.9	44.4
104.5	97.9	37.4
105.8	97.9	44.4
103.2	95.3	45.0
104.5	96.6	44.7
107.1	99.2	44.0
105.8	97.9	44.4
103.2	96.6	37.4
Avg 105.0	97.4	42.7

Table 3.9 Mobilization pressures for hexadecane in an oil-wet capillary tube, obtained from buret volume and head of water in reservoir.

Volume (ml)	Head of Water (mm)	Pressure (Pa)
22.0	5.25	51.4
21.2	5.06	49.6
21.9	5.23	51.2
21.9	5.23	51.2
21.0	5.01	49.1
19.9	4.75	46.5
19.2	4.58	44.9
18.5	4.42	43.2
20.3	4.85	47.5
20.2	4.82	47.2
20.8	4.97	48.6
19.7	4.71	46.1
20.4	4.87	47.7
21.2	5.06	49.6
20.7	4.95	48.4
20.8	4.97	48.6
21.2	5.06	49.6
21.6	5.16	50.5
21.6	5.16	50.5
21.5	5.14	50.3
20.9	4.99	48.9
21.9	5.23	51.2
21.8	5.21	51.0
	Avg	48.8

Table 3.10 Mobilization pressures for hexadecane in an oil-wet capillary tube, obtained from contact angle measurements.

Advancing Contact Angle θ_{Awo} (degrees)	Receding Contact Angle θ_{Row} (degrees)	Pressure (Pa)
156.9	158.8	56.4
158.8	127.8	55.6
158.0	124.8	61.9
158.5	126.2	59.1
154.8	128.2	49.9
Avg 157.4	126.7	56.6

Table 3.11 Mobilization pressures for hexadecane-air in an oil-wet capillary tube, obtained from buret volume and head of water in reservoir.

Volume (ml)	Head of Water (mm)	Pressure (Pa)
23.9	5.71	55.9
23.7	5.66	55.4
22.9	5.47	53.5
23.1	5.52	54.0
23.4	5.59	54.7
23.0	5.49	53.8
22.8	5.45	53.3
23.1	5.52	54.0
23.3	5.57	54.5
22.5	5.37	52.6
22.6	5.40	52.8
22.4	5.35	52.4
22.9	5.47	53.5
22.0	5.26	51.4
21.6	5.16	50.5
21.8	5.19	51.0
21.5	5.14	50.3
21.7	5.18	50.7
21.7	5.18	50.7
21.5	5.14	50.3
21.2	5.06	49.6
21.4	5.11	50.0
21.4	5.11	50.0
21.2	5.06	49.6
21.0	5.01	49.1
21.7	5.18	50.7
21.5	5.12	50.3
21.1	5.04	49.3
21.3	5.09	49.8
21.9	5.23	51.2
	Avg	51.8

Table 3.12 Mobilization pressures for hexadecane-air in an oil-wet capillary tube, obtained from contact angle measurements.

Contact Angles for Hexadecane/Water (degrees)		Contact Angles for Hexadecane/Air (degrees)			Pressure (Pa)
θ_{Awo}	θ_{Row}	θ_{Aog}	θ_{Rgo}		
152.0	123.4	16.9	15.4		58.6
153.7	122.4	14.7	13.3		63.5
156.1	122.7	15.9	11.7		67.5
152.4	123.2	15.2	13.8		59.8
159.3	123.4	18.4	16.2		68.8
157.7	124.0	17.0	14.8		65.0
155.3	121.3	16.2	14.0		68.9
155.2	122.9	16.3	14.2	Avg	64.5

Chapter 4 Glass Micromodel Experiments

4.1 Description of Apparatus

The glass micromodel of pores and throats was fused together in order to accurately measure the pressure drop across the different phases. A serious drawback associated with the fusion process was the difficulty in keeping the model clean during the water-wet experiments. Contamination was minimized by using the following sequence for the experiments :

i) with the model initially water-wet, the pressure required to mobilize discrete, discontinuous air bubbles through the model was measured;

ii) as in i) but with hexadecane as the discontinuous, nonwetting phase to be displaced;

iii) as in i) but with hexadecane and air as the discontinuous, nonwetting phases to be displaced;

iv) the wetting condition of the model was altered by coating the pore and throat surfaces with a siliconizing agent (Surfasil), and repeating the three phases to be displaced, i.e. air, hexadecane and hexadecane/air.

Water wettability was maintained for the initial series of water-wet experiments by flushing the model with 1 M NaOH solution prior to experimentation and by storing the model with NaOH solution.

The model was drilled with an inlet and an outlet port prior to fusion, by which fluids could be introduced into the model. The ends of the upstream and downstream water reservoirs had Swage-Lok fittings equiped with O-ring seals, and were attached to the model with clamps. Water flow from the upstream or inlet side was controlled by a two-way stopcock. Pressure was applied to the phase being mobilized by either raising the upstream reservoir relative to the

model (and downstream reservoir) or by the addition of water to the upstream reservoir from a calibrated buret (Figure 9).

The applied head was measured on a vertical scale whose smallest divisions were given in millimetres; or by calculating the rise in height of the water level in the water reservoir from the volume added by the buret and the measured diameter of the reservoir container. The displacement of the different phases was viewed through a 35 millimetre camera with an attached bellows and closeup lens, mounted above the model. The micromodel was placed on a ground glass plate which allowed diffuse illumination from a high intensity light source for photographing the displacement mechanisms.

4.2 Experimental Procedure

Water-wet experiments were performed in the following manner : The glass micromodel is flushed of its storage solution with quartz distilled water. Approximately 20 ml of fresh NaOH solution is flushed through the model followed by additional distilled water. The model is left with all elements (pores, throats and moats) water-filled. Air is drawn into the model for the first series of water-wet experiments, either through the inlet or outlet moat, since the flow direction is alternated to negate the effects of directional heterogeneity on mobilization pressure. Bubbles which were displaced in the sequence from P1 toward P10 were considered as having been mobilized in the "normal" direction; bubbles displaced in the opposite sense, from P10 to P1, are mobilized in the "reverse" direction.

Air is nonwetting and enters the pores as small discrete bubbles which quickly coalesce to form large bubbles and eventually fill the entire pore. The number of pores which are air-filled vary from three to seven. The integrity of a

Figure 9. Apparatus for measuring mobilization pressure in glass micromodel experiments.

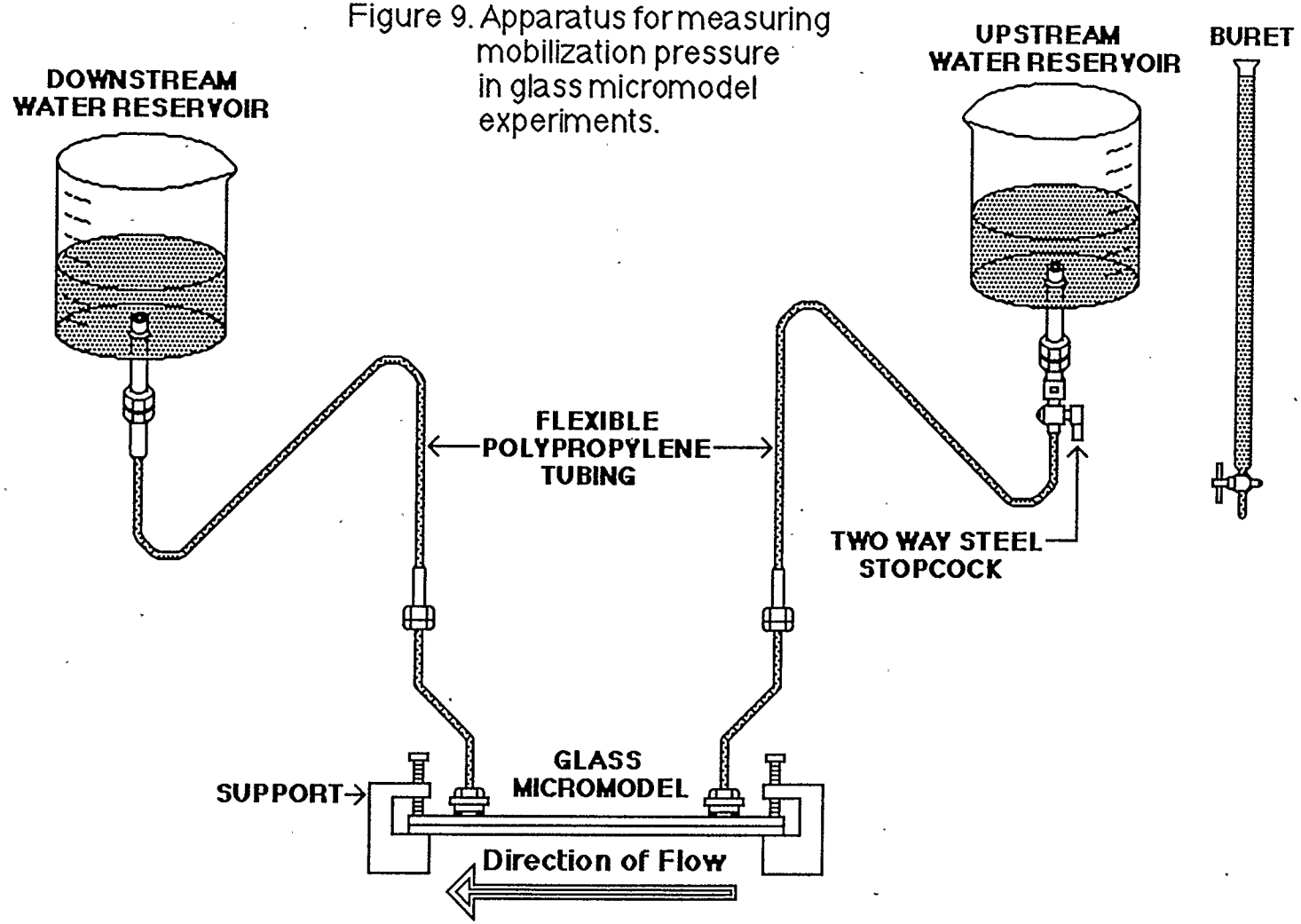

single air-filled pore proved difficult to maintain when the water reservoirs were attached to the model. There was a sharp pressure imposed on the model as the clamp was fastened which caused the single air bubble to fission into three or more smaller bubbles into adjoining pores. Three or more air-filled bubbles resisted this sharp change in pressure such that the bubbles were not significantly affected (i.e. only a small portion of an end bubble would lose some of its volume to the adjacent empty pore).

The attached water reservoirs are positioned such that their water levels are at the same elevation. The upstream reservoir is clamped to a height adjustable stand which allowed it to be raised or lowered. Pressure is imposed on the phase to be displaced by moving the upstream reservoir upward. When mobilization seems imminent, the means of applying pressure is switched to the buret, allowing the water level to rise but not jarring the tubing attached to the model and inadvertently and prematurely mobilizing the bubbles. Mobilization occurs when the leading interface between water and air enters the throat on the downstream end, and suddenly moves into the pore located downstream. The air filled pore furthest downstream shows the greatest development of a finger of air into its downstream throat and is the first to be mobilized. The hexadecane and hexadecane/air experiments in the water-wet micromodel are accomplished in the same manner, with the hexadecane being introduced into the model from a glass Multifit syringe.

Oil-wet experiments follow the completion of the water-wet experiments. Sufasil is injected into the model and flushed through after about 15 minutes. The Surfasil is drained from the model by a continuous stream of air followed by suction with a vacuum line. The model is then placed in an oven to bake for 10 minutes at 120 ^{o}C. It was easier to maintain the integrity of a single bubble of

air, hexadecane or hexadecane/air under oil-wetting conditions than water-wet. In experiments where air and water were involved, both phases were essentially intermediately wetting the glass surface; in experiments where hexadecane and hexadecane/air were the phases to be displaced, hexadecane contacted the surface and attachment of the reservoirs failed to fission the wetting phase. The method of pressure measurement involved the addition of water to the upstream reservoir from the calibrated buret rather than elevating it because much less pressure was required to mobilize the single bubble.

In water-wet experiments, all three displaced phases were nonwetting with respect to the glass surface, therefore they all assumed a position in the central portion of the pores, while water formed a thin film around them and occupied the narrower throats (Figure 10). However, in the oil-wet experiments, the difference in the wetting characteristics of the phases, resulted in different positions for maximum mobilization pressures (Figure 11). When air is being displaced, its position of maximum pressure occurs in a manner similar to that for water-wet, except the finger of air is fully in the downstream throat. For hexadecane as the displaced phase, its position of maximum pressure has its leading interface contained within the pore and its trailing interface in the upstream throat. The hexadecane/air phases exhibit both the hexadecane only and air only behaviour. Initially, the interfaces are the same as those for hexadecane only, i.e. leading interface in pore and trailing interface in upstream throat. However, as hexadecane is stripped away from the upstream end and moved to the downstream side, the combined hexadecane/air bubble assumes a configuration similar to that for air only in an oil-wet system, i.e. leading interface fully in downstream throat while the trailing interface remains in the pore.

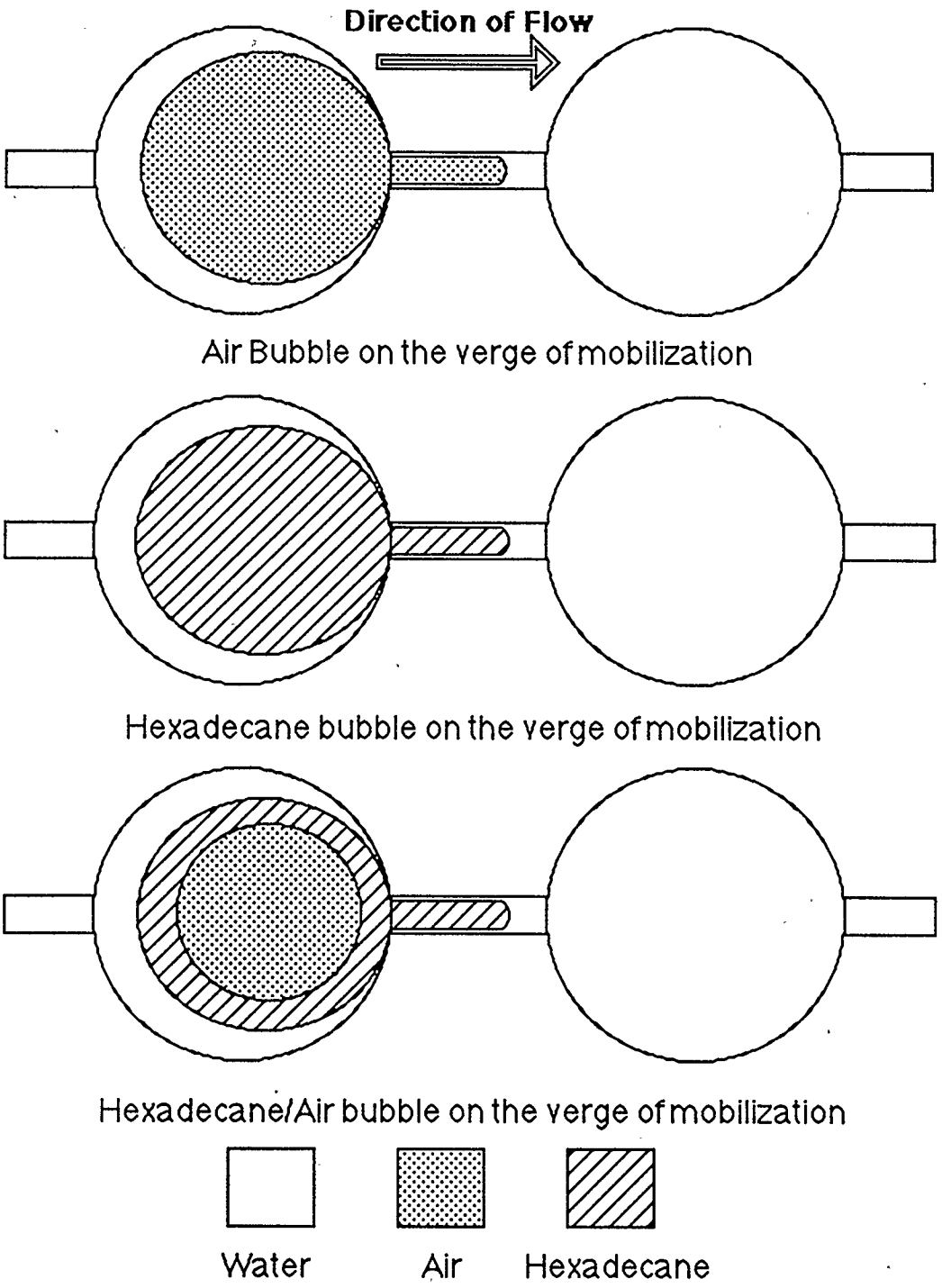

Figure 10. Configuration of displaced phases in a water-wet micromodel system.

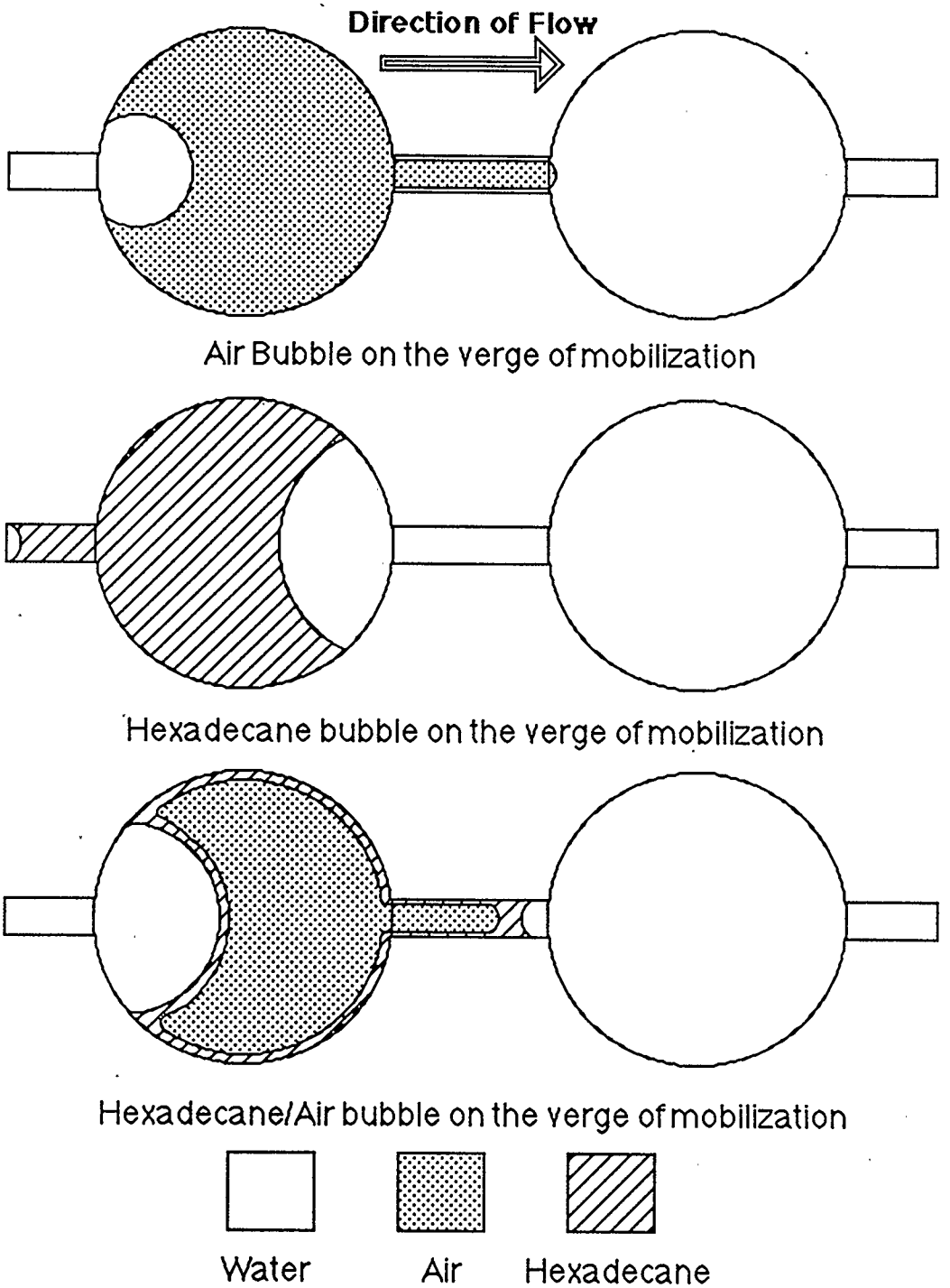

Figure 11. Configuration of displaced phases in an oil-wet micromodel system.

4.3 Experimental Data

For water-wet experiments, the mobilization pressures are determined from the difference in height of the water levels in the upstream (elevated) and downstream reservoirs :

$$P = \rho g h \qquad \text{(Eqn. 4.1)}$$

where ρ = the density of water

g = the acceleration due to gravity

h = the difference in elevation between reservoirs

Tables 4.1, 4.2 and 4.3 give the direction of flow, the number of bubbles of displaced phase(s), the head of water required to mobilize them, the total pressure and the mobilization pressure for a single bubble, for experiments where the displaced phases are air, hexadecane and hexadecane/air, respectively, and the displacing phase is water. Plates 4, 5 and 6 illustrate the mobilization of air, hexadecane and hexadecane/air, respectively, in a water-wet micromodel.

For oil-wet experiments, the mobilization pressures are determined from the calculated surface area of the water reservoir and the measured volume of water added by the buret, in a manner previously used for the oil-wet capillary tube experiments. The water reservoir is of circular cross-section with a diameter of 7.30 centimetres. The pressures can be calculated from the geometry of simple solids (a cylinder) :

$$V = \pi r^2 h \qquad \text{(Eqn. 4.2)}$$

and hydrostatic head :

$$P = \rho g h$$

Tables 4.4, 4.5 and 4.6 give the direction of flow, volume added, head and mobilization pressures for experiments where the displaced phases are air,

Table 4.1 Mobilization pressures for air in a water-wet micromodel, obtained from the head difference between the upstream and downstream water reservoirs.

Flow direction (normal or reverse)	Number of Pores filled by air	Head of Water (cm)	Total Pressure (Pa)	Pressure/Pore (Pa)
n	4	22.2	2172.4	543.1
n	5	30.6	2994.4	598.9
n	6	36.2	3542.3	590.4
n	7	42.8	4188.2	598.3
r	4	24.8	2426.8	606.7
r	4	25.2	2465.9	616.5
r	5	31.6	3092.2	618.4
r	6	38.5	3767.4	627.9
r	7	43.8	4286.0	612.3
			Avg	601.4

Table 4.2 Mobilization pressures for hexadecane in a water-wet micromodel, obtained from the head difference between the upstream and downstream water reservoirs.

Flow direction (normal or reverse)	Number of Pores filled by hexadecane	Head of Water (cm)	Total Pressure (Pa)	Pressure/Pore (Pa)
n	3	11.7	1144.9	381.6
n	4	14.3	1399.3	349.8
n	5	17.9	1751.6	350.3
n	6	22.8	2231.1	371.8
n	7	25.9	2534.4	362.1
r	4	14.4	1379.8	344.9
r	4	14.5	1418.9	354.7
r	5	18.4	1800.5	360.1
r	6	20.3	1986.4	331.1
r	7	26.0	2544.2	363.5
			Avg	357.0

Table 4.3 Mobilization pressures for hexadecane/air in a water-wet micromodel, obtained from the head difference between the upstream and downstream water reservoirs.

Flow direction (normal or reverse)	Number of pores	Phase(s) mobilized	Head of Water (cm)	Total Pressure (Pa)	Pressure/Pore (Pa)
n	4	Hex	14.2	1389.5	347.4
		Hex/Air	31.4	3072.6	768.2
n	4	Hex	14.3	1399.3	349.8
		Hex/Air	30.3	2935.6	733.9
n	5	Hex	18.6	1820.1	364.0
		Hex/Air	39.7	3884.8	776.9
n	6	Hex	21.3	2084.3	347.4
		Hex/Air	38.6	3777.2	629.5
n	7	Hex	27.1	2651.8	378.8
		Hex/Air	46.9	4589.4	655.6
r	4	Hex	15.1	1477.6	369.4
		Hex/Air	33.6	3287.9	822.0
r	5	Hex	16.8	1643.9	328.8
		Hex/Air	38.5	3767.4	753.5
r	6	Hex	21.2	2074.5	345.8
		Hex/Air	41.0	4012.0	668.7
r	7	Hex	30.7	3004.1	429.1
		Hex/Air	46.6	4560.0	651.4
				Avg (Hex)	362.3
				Avg (Hex/Air)	717.7

Plate 4

Glass micromodel, water-wet, displaced phase is air, displacing phase is water. Air is the dark outlined phase occupying the pore spaces. The direction of flow is indicated by the arrows. The sequence of photographs shows the leading interfaces of the air bubble in the downstream throats and the trailing interfaces in the pore body. Mobilization pressure is 601 Pa.

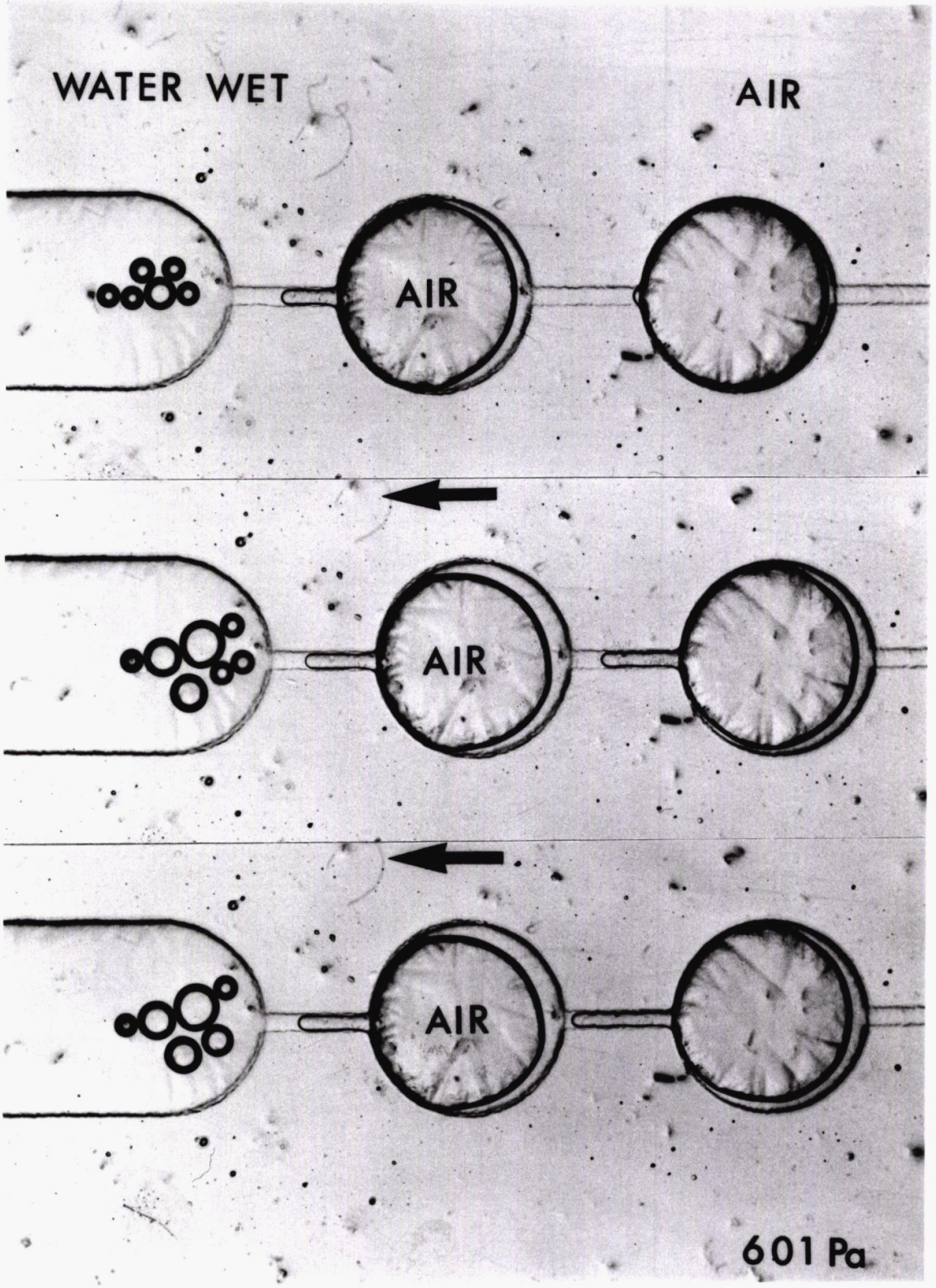
WATER WET
AIR
AIR
AIR
AIR
601 Pa

Plate 5

Glass micromodel, water-wet, displaced phase is hexadecane, displacing phase is water. Hexadecane occupies the pore spaces. The direction of flow is indicated by the arrows. The sequence of photographs shows the leading interfaces of the hexadecane bubble in the downstream throats and the trailing interfaces in the pore body. Mobilization pressure is 357 Pa.

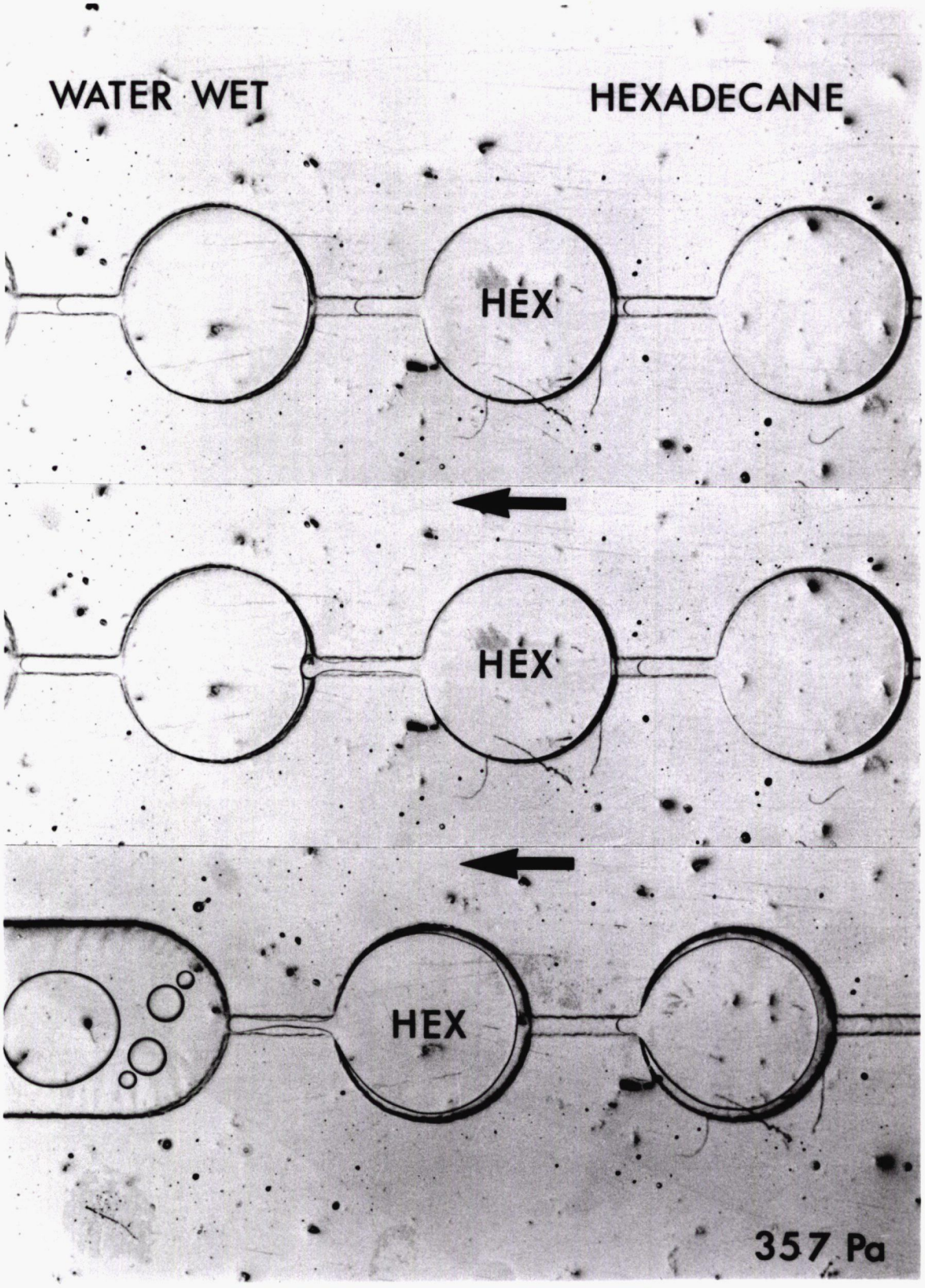
WATER WET
HEXADECANE
HEX
HEX
HEX
357 Pa

Plate 6

Glass micromodel, water-wet, displaced phase is hexadecane/air, displacing phase is water. Air is the dark outlined phase surrounded by hexadecane, both phases occupy the pore spaces. The direction of flow is indicated by the arrows. The sequence of photographs shows the initial mobilization of excess hexadecane at the lower pressure of 362 Pa, followed by the mobilization of the combined hexadecane/air bubble at 718 Pa. Note that the leading interfaces of the nonwetting phases are present in the downstream throats and the trailing interfaces in the pore body.

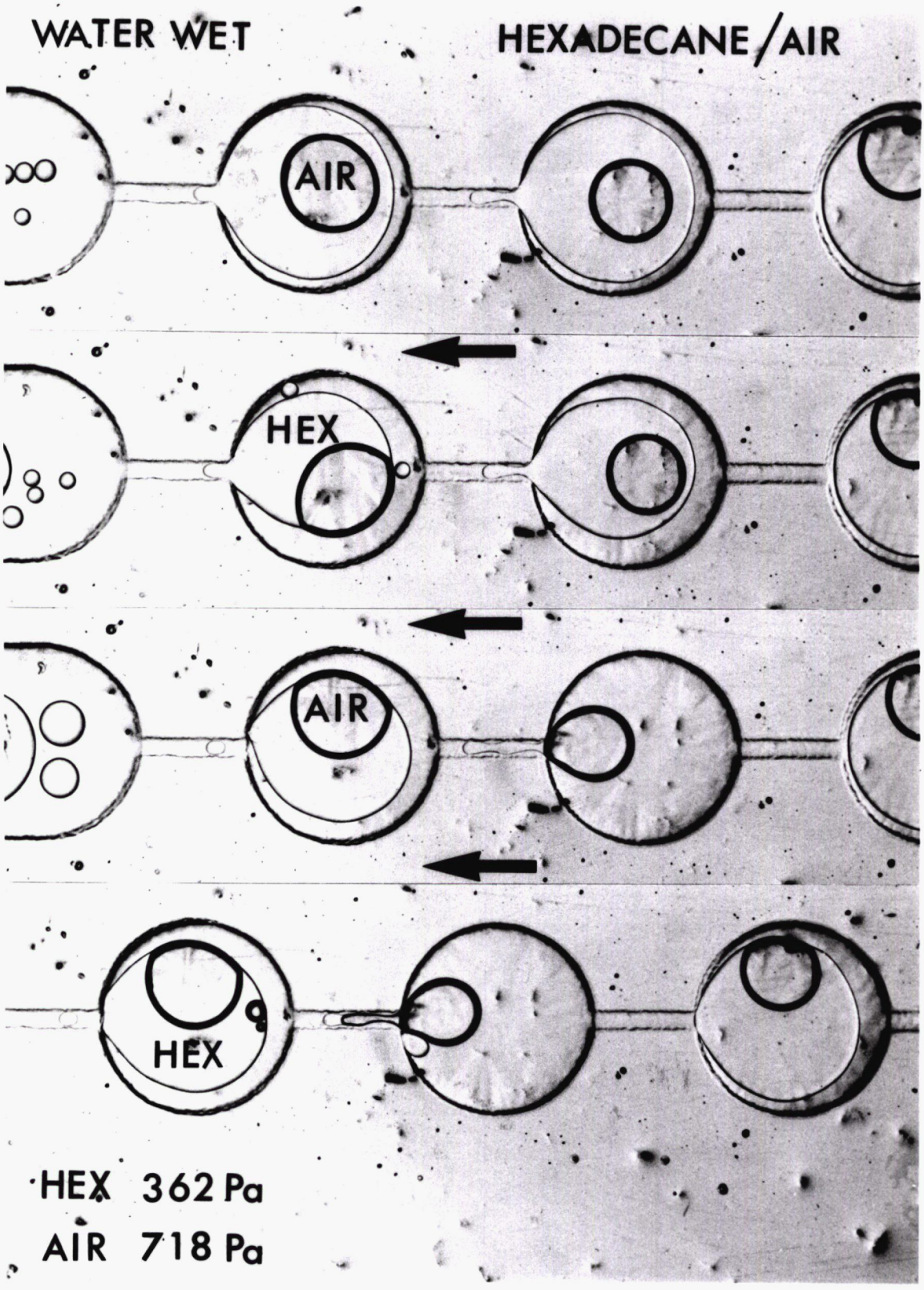
WATER WET
HEXADECANE/AIR
AIR
HEX
AIR
HEX
HEX 362 Pa
AIR 718 Pa

Table 4.4 Mobilization pressures for air in an oil-wet micromodel, obtained from buret volume and head of water in reservoir.

Flow direction (normal or reverse)	Volume (ml)	Head of Water (cm)	Pressure (Pa)
n	229.9	5.5	536.8
n	200.0	4.8	467.0
n	190.7	4.6	445.3
n	258.2	6.2	603.9
n	247.1	5.9	577.7
r	224.6	5.4	524.5
r	191.5	4.6	447.2
r	200.0	4.8	467.0
r	189.3	4.5	442.0
		Avg	501.3

Table 4.5 Mobilization pressures for hexadecane in an oil-wet micromodel, obtained from buret volume and head of water in reservoir.

Flow direction (normal or reverse)	Volume (ml)	Head of Water (cm)	Pressure (Pa)
n	244.7	5.8	572.1
n	258.7	6.2	604.8
n	249.9	6.0	584.3
n	250.0	6.0	584.5
n	260.8	6.2	609.7
r	261.9	6.3	612.3
r	250.0	6.0	584.5
r	250.0	6.0	584.5
r	262.8	6.3	614.4
r	254.0	6.1	593.8
r	259.4	6.2	606.5
r	250.0	6.0	584.5
r	254.4	6.1	594.8
r	247.8	5.9	579.4
		Avg	593.6

Table 4.6 Mobilization pressures for hexadecane/air in an oil-wet micromodel, obtained from buret volume and head of water in reservoir.

Flow direction (normal or reverse)	Volume (ml)	Head of Water (cm)	Pressure (Pa)
n	296.8	7.1	693.9
n	300.0	7.2	701.4
n	300.0	7.2	701.4
n	306.0	7.3	715.4
n	280.6	6.7	656.0
n	297.1	7.1	694.6
n	283.1	6.8	661.9
n	300.0	7.2	701.4
n	300.0	7.2	701.4
n	279.8	6.7	654.2
r	295.8	7.1	691.6
r	300.0	7.2	701.4
r	314.5	7.5	735.3
r	300.0	7.2	701.4
r	302.8	7.2	707.9
r	309.4	7.4	723.4
r	306.8	7.3	717.3
r	312.7	7.5	731.1
r	298.9	7.1	698.8
r	298.4	7.1	697.7
		Avg	699.4

hexadecane and hexadecane/air, respectively, and the displacing phase is water. Plates 7, 8 and 9 illustrate the mobilization of air, hexadecane and hexadecane/air, respectively, in an oil-wet micromodel.

Plate 7

Glass micromodel, oil-wet, displaced phase is air, displacing phase is water. Air is the dark outlined phase occupying the pore spaces. The direction of flow is indicated by the large arrows. The sequence of photographs shows the leading interface of the air bubble in the downstream throat and the trailing interface in the pore body. Mobilization pressure is 501 Pa.

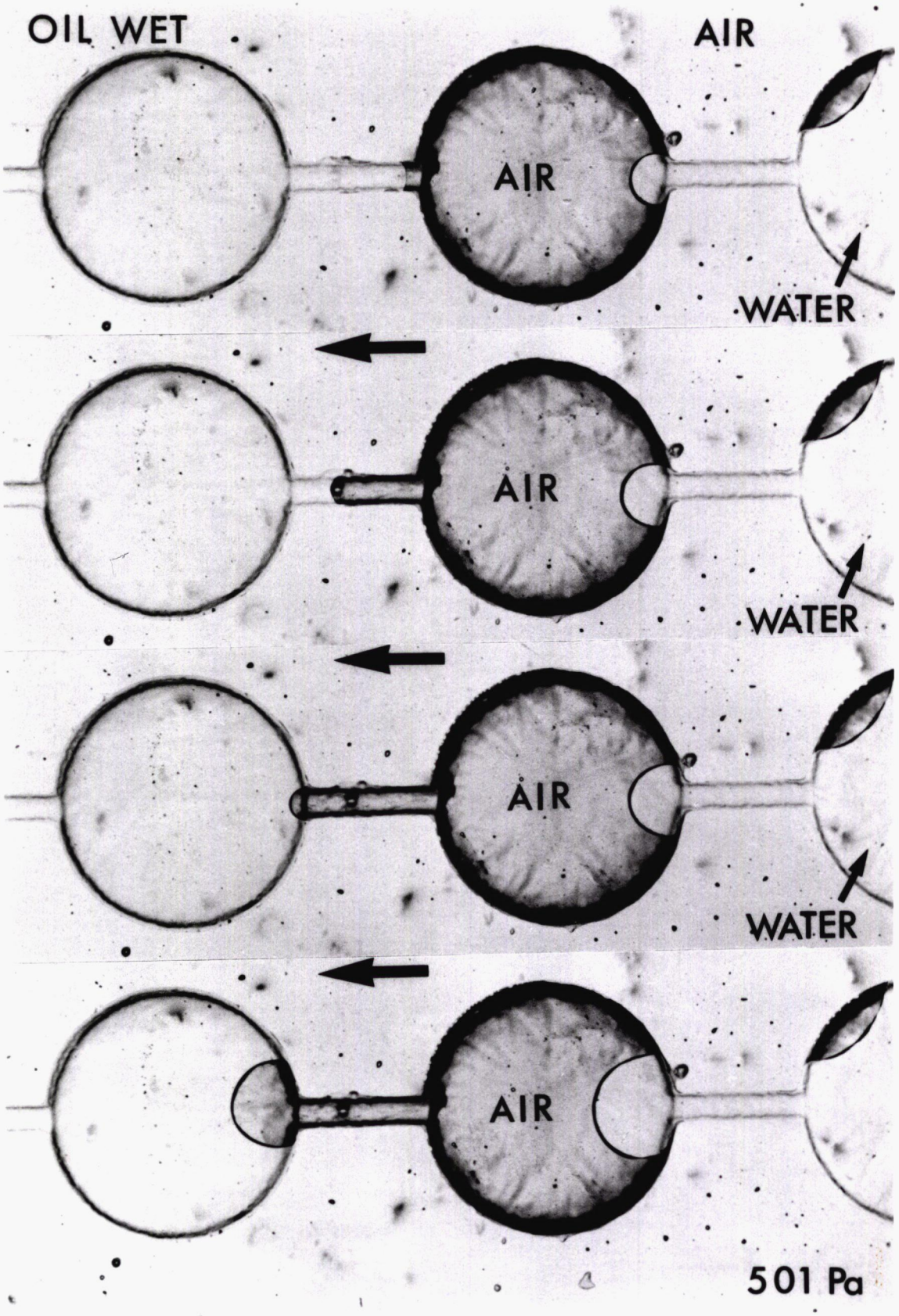
OIL WET
AIR
AIR
WATER
AIR
WATER
AIR
WATER
AIR
501 Pa

Plate 8

Glass micromodel, oil-wet, displaced phase is hexadecane, displacing phase is water. Water is the outlined phase, hexadecane has nearly the same refractive index as the glass and coats the pore and throat walls. The direction of flow is indicated by the large arrows. The sequence of photographs shows the leading interface of the hexadecane phase in the pore body and the trailing interface in the upstream throat . Mobilization pressure is 594 Pa.

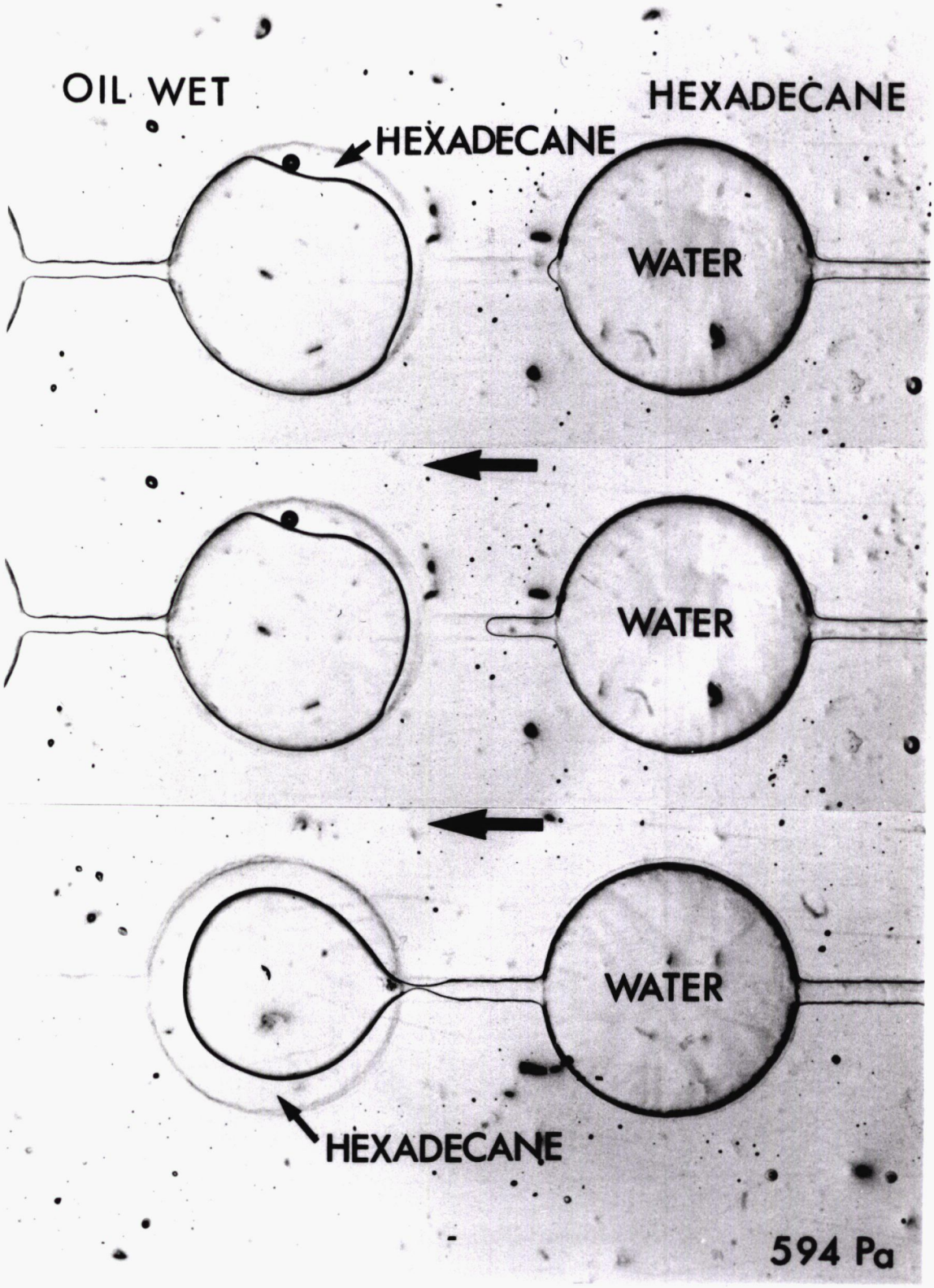
OIL WET
HEXADECANE
HEXADECANE
WATER
WATER
WATER
HEXADECANE
594 Pa

Plate 9

Glass micromodel, oil-wet, displaced phase is hexadecane/air, displacing phase is water. Air is the dark outlined phase surrounded by hexadecane which also occupies the downstream throat. The direction of flow is indicated by the large arrows. The sequence of photographs shows the initial mobilization of excess hexadecane at a lower pressure, followed by the mobilization of the combined hexadecane/air bubble at 699 Pa.

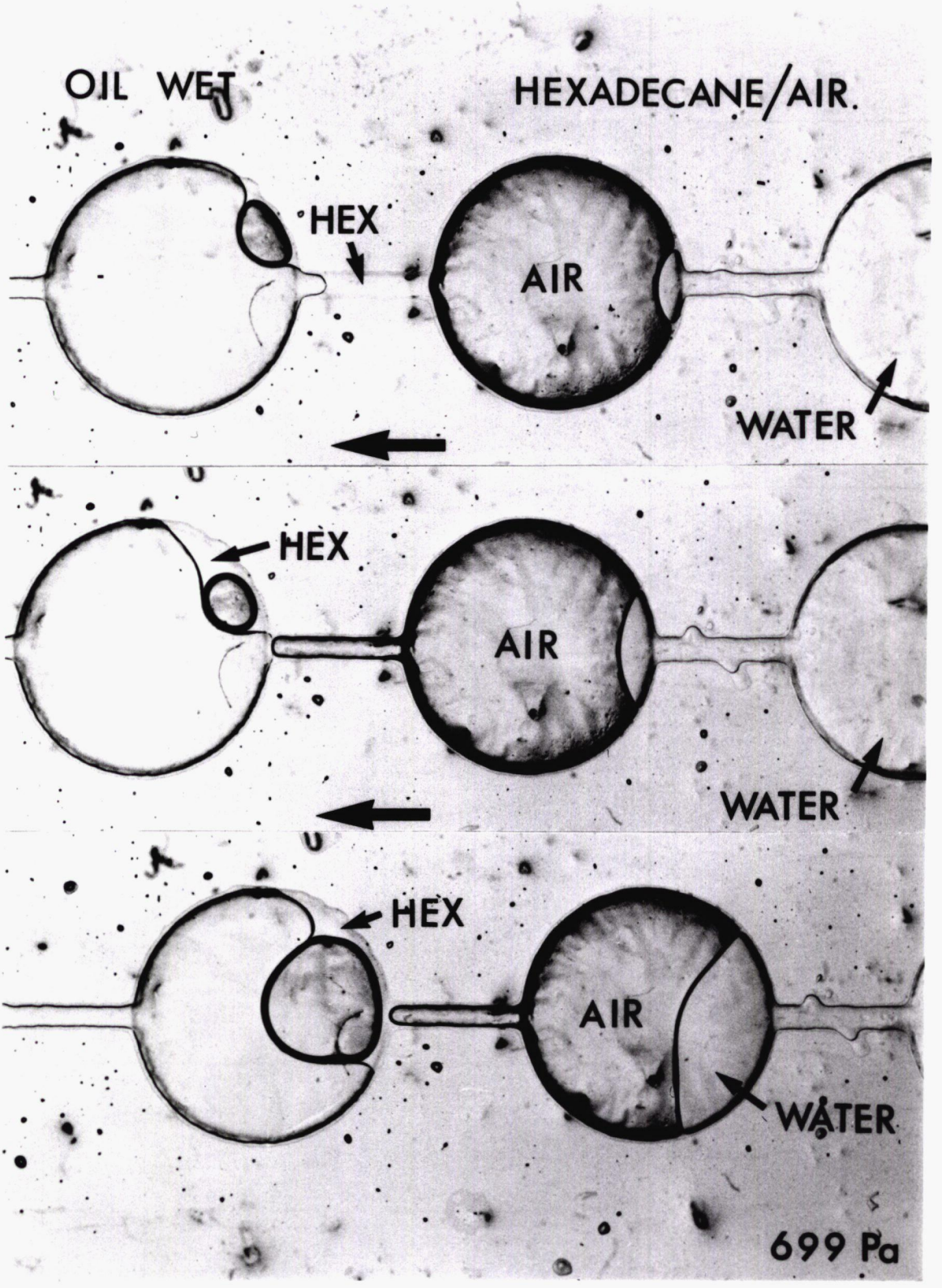
OIL WET
HEXADECANE/AIR.
HEX
AIR
WATER
HEX
AIR
WATER
HEX
AIR
WATER
699 Pa

Chapter 5 Discussion

5.1 Discussion of Capillary Tube Results

Results for the capillary tube experiments are presented in Figure 12. The displaced phases were air, hexadecane and hexadecane/air respectively, while the displacing phase, in all instances, was water. The wettability of the capillary tubes was either water-wet ($\theta_E \sim 0°$) or oil-wet ($\theta_E \sim 150°$).

The following information is provided for each type of capillary tube experiment:

i) the average measured pressure (M) required to mobilize the bubble;

ii) the average advancing and receding contact angles for the different bubble phases;

iii) the average mobilization pressure (C) calculated from contact angle hysteresis;

iv) the observed configuration of the different phases within the confines of the capillary; and

v) the pressure profile across the various interfaces.

The Jamin resistance to flow in capillary tubes of constant cross-section is caused by the hysteresis between the advancing and receding contact angles which is influenced by wettability and surface roughness. Gardescu (1930) determined that the pressure drop required to mobilize a bubble of air in a wetted capillary tube is independent of the length of the bubble since it results only from the boundary conditions at the two extremities of the bubble.

The diagrammatic pressure profiles show the pressure changes across the various bubble interfaces and also the additive and subtractive nature of combining different configurations. As an example, under water-wet conditions,

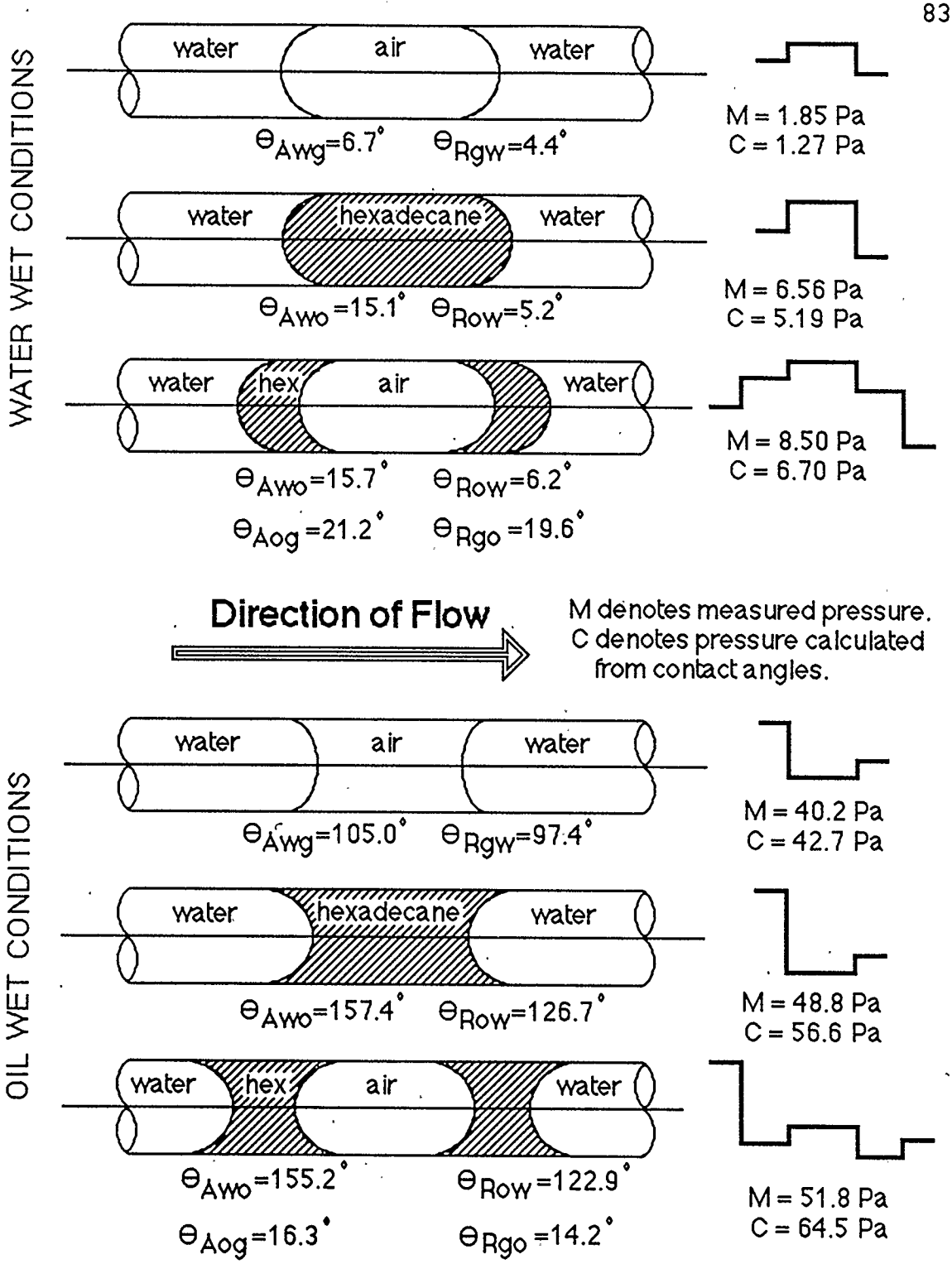

Figure 12. Results from capillary tube experiments.

the sum of pressures for mobilizing air and hexadecane individually is nearly of the same magnitude as that for the combined hexadecane/air bubble, 8.41 Pa vs. 8.50 Pa. A second example involves adding the pressure required for the air bubble under water-wet conditions to that for the hexadecane under oil-wet conditions. This compares with the combined hexadecane/air bubble under oil-wet conditions (50.6 Pa vs. 51.8 Pa).

Therefore, the resistance to flow by discrete and discontinuous bubbles in a capillary of uniform diameter and cross-section is a function of the number of pairs of interfaces within the capillary. The pressure required to mobilize these bubbles depends on contact angle hysteresis. The bubbles will be mobilized when the maximum advancing and receding contact angles associated with the trailing and leading interfaces are achieved. In cylindrical capillary tubes, depending on the types of displaced and displacing phases, these contact angles are a function of surface roughness and system wettability.

Morrow (1975) defined three classes of behaviour in polytetrafluoroethylene (PTFE) capillary tubes relating contact angle hysteresis and surface roughness. A comparison of the measured advancing and receding contact angles with Morrow's criteria suggests that the glass tubes used approximate Class II type behaviour (i.e. advancing and receding angles are about 12 ± 5 degrees respectively, higher and lower than that of the intrinsic angle).

The combined Laplace-Young equation of capillarity gives the pressure for the mobilization of a blob of a single phase as : $P_c = [2\gamma / r] (\cos \theta_R - \cos \theta_A)$. Therefore, pressure is directly proportional to the difference of the cosines of the receding and advancing contact angles. It is therefore possible to compare the effects of wettability on mobilization pressure except for the case where the

displaced phase is air. Under water-wet conditions, air is clearly the nonwetting phase but, in the siliconized capillary tubes, neither air nor water wet the glass surface and an intermediate wetting condition exists, which is unlike the other cases where one phase is clearly nonwetting and the other, wetting.

Table 5.1 presents the differences (δ) between the cosines of the measured receding and advancing angles for both water-wet and oil-wet conditions. The displacement of air, hexadecane and hexadecane/air by water in all cases in the oil-wet system can be compared to the displacement of the same phases in the water-wet system by dividing the difference of cosines for oil-wet conditions ($\delta_{oil\text{-}wet}$) by the difference of cosines for water-wet ($\delta_{water\text{-}wet}$). This dimensionless ratio (ε) is a measure of how much more difficult it is to mobilize a discontinuous oil or oil-gas phase in a cylindrical capillary tube under oil-wet conditions than under water-wet conditions. From measured advancing and receding angles, when hexadecane is the displaced phase, ε is 10.7; for hexadecane/air, ε is 11.6. Contact angle hysteresis increases with increasing intrinsic contact angle (θ_E). Greater hysteresis exists in oil-wet systems because these systems have larger intrinsic contact angles ($105° < \theta_E < 180°$) than water-wet systems ($0° < \theta_E < 75°$) (Anderson, 1986); consequently, higher pressure gradients are necessary to mobilize wetting phases.

Based on measured pressures (as opposed to the pressures calculated from measured contact angles), ε for hexadecane is 7.44; for hexadecane/air, ε is 6.09. This discrepancy arises from the different methods by which mobilization pressures are measured and the means by which contact angles are calculated from measurements taken from photographs. The measurements for determining contact angles is exceedingly sensitive to error propagation with a corresponding loss in the degree of precision. Mobilization pressures were

Table 5.1 A comparison of the water-wet and oil-wet capillary tube systems from the difference of the cosines of the advancing and receding contact angles.

Notes : 1) Water is the displacing phase in all cases.
2) For the displaced phase Hexadecane/Air, only the advancing and receding contact angles between Hexadecane and water are used in the calculation of δ.

Water-wet Capillary Tubes

Displaced Phase	θ_R	cos θ_R	θ_A	cos θ_A	$\delta_{water\text{-}wet}$
Air	4.4	0.9971	6.7	0.9932	0.0039
Hexadecane	5.2	0.9959	15.1	0.9655	0.0304
Hexadecane/Air	6.2	0.9942	15.7	0.9627	0.0315

Siliconized ("Oil-wet") Capillary Tubes

Displaced Phase	θ_R	cos θ_R	θ_A	cos θ_A	$\delta_{oil\text{-}wet}$
Air	97.4	-0.1288	105.0	-0.2588	0.1300
Hexadecane	126.7	-0.5976	157.4	-0.9232	0.3256
Hexadecane/Air	122.9	-0.5432	155.2	-0.9078	0.3646

Phases	Water/Air	Water/Hexadecane	Water/(Hexadecane/Air)
Epsilon (ε)	33.49 †	10.71	11.59

Where $\delta = (\cos\theta_R - \cos\theta_A)$

$\varepsilon = (\delta_{oil\text{-}wet}) / (\delta_{water\text{-}wet})$

† Not directly comparable (neither air nor water are wetting in siliconized tubes)

measured for capillary tube experiments by two methods : for water-wet tubes, the lower pressures required for mobilization necessitated the use of the tilt angle method; for oil-wet tubes, water was added to the upstream water reservoir by means of a calibrated buret. Both of these methods are much less sensitive to error propagation than pressures calculated from the measured contact angles.

Results obtained from this study are consistent with published literature. Smith and Crane (1930) performed similar experiments on straight, uniform diameter capillaries for an "uncontaminated" tube (essentially a tube cleaned with hot chromic acid, rendering it water-wet) and tubes contaminated with oleic acid in benzene (making them intermediate to oil-wet). They concluded that the Jamin resistance in a capillary where the fluid completely wetted the surface could not sustain any pressure. An analysis of their data indicates that, in experiments where a series of air bubbles were contained in an uncontaminated capillary with radius of 540 microns, the average pressure sustained by each bubble was 1.90 Pa. In similar experiments with air as the displaced phase in a water-wet tube, the average measured pressure after adjusting for the different tube radius is 1.48 Pa. In Smith and Crane's contaminated tube experiments, two different concentrations of oleic acid were used and greater resistance accompanied the lower concentration. They postulated that the excess oleic acid in the higher concentration experiments was adsorbed on the water-air interface, effectively reducing the surface tension. Regardless, the overall average pressure sustained by each bubble was 55.5 Pa. Because of the excess oleic acid present at the water-air interfaces, this may be considered to be equivalent to that for experiments where hexadecane/air is the displaced phase(s) in an oil-wet system. After

adjusting for the different radii, the measured pressure is 41.3 Pa.

A study by Schwartz et al (1964) attempted to define the resistance of a liquid-solid-vapour boundary line as it is being moved along the solid surface in capillary systems where the contact angle is substantially greater than zero. This resistance was characterized and defined as the critical line force (CLF). In a comparison of one of their experiments with an equivalent system where air is the displaced phase and water the displacing phase on an intermediate wetted capillary surface, Schwartz et al determined a CLF for the resistance caused by the set of interfaces for water and air as ranging from 13.6 to 14.0 mN/m. The equivalent calculation, after adjusting for the different radii gives a CLF of 9.9 to 10.6 mN/m. Schwartz et al suggest that the contact angle hysteresis on all surfaces would reach a maximum at $\theta_E = 90°$. The capillary tube experiments for this study indicate otherwise; that maximum contact angle hysteresis will increase with increasing intrinsic contact angle.

5.2 Discussion of glass micromodel experiments

Results from glass micromodel experiments are presented in Figure 13. The displaced phases are air, hexadecane and hexadecane/air respectively, while the displacing phase, in all instances, was water. The wettability of the micromodel was initially water-wet ($\theta_E \sim 0°$) and at the conclusion of water-wet experiments was altered with a siliconizing agent to behave in an oil-wet manner when hexadecane and hexadecane/air are the displaced phases ($\theta_E \sim 150°$).

The information provided in Figure 13 is similar to that given for capillary tube experiments except that contact angles could not be measured directly within the micromodel system. Therefore, considering that the same fluids were

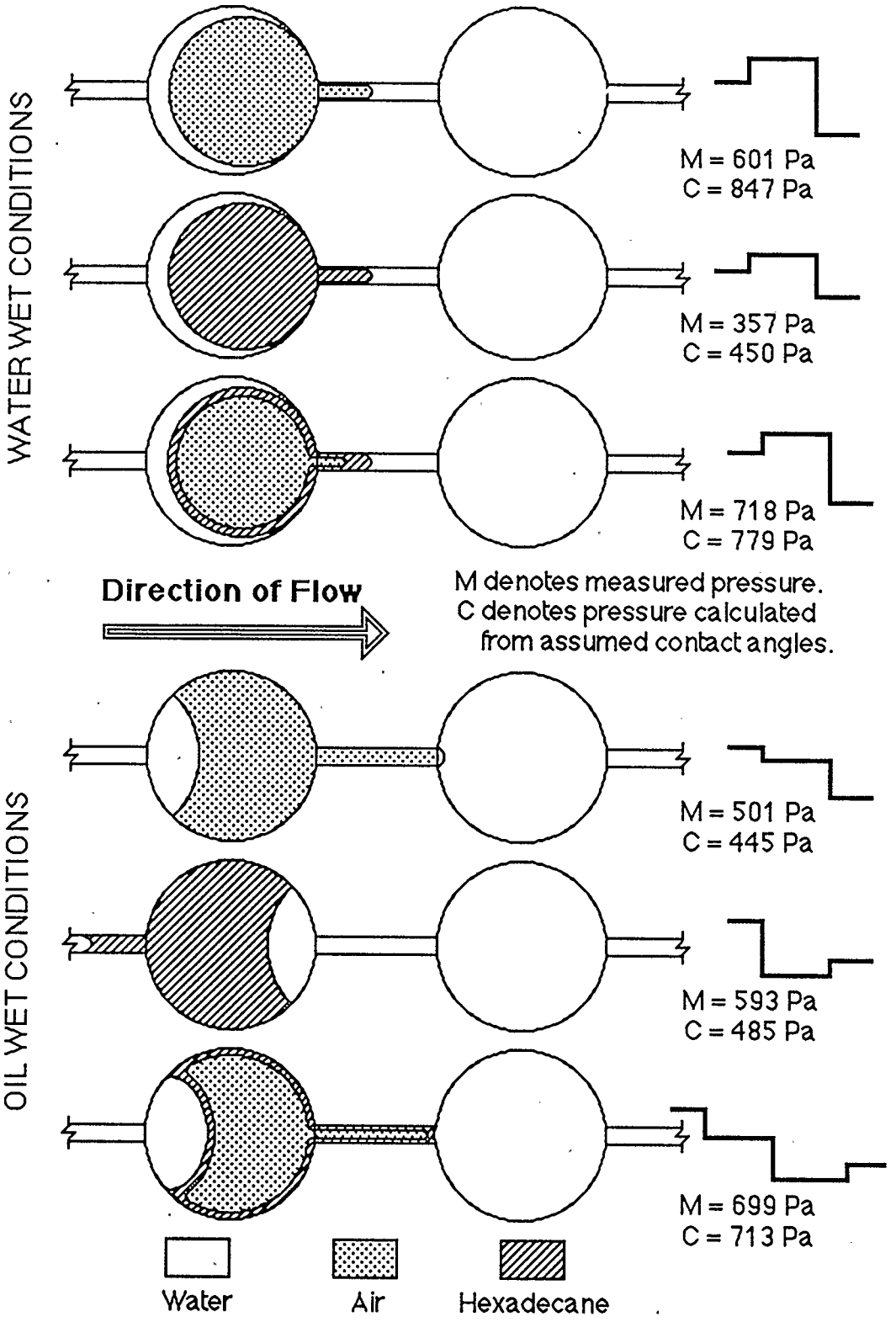

Figure 13. Results from glass micromodel experiments.

used, and glass surfaces were involved in both series of experiments, it was assumed that displacement of the different phases involved the same advancing and receding contact angles. Since the micromodel was not fabricated from the same type of glass as the capillary tubes and the etching and fusing process may have affected the surface roughness of the model, it is possible that the surfaces may differ and have different effects on contact angle hysteresis. Another factor to be considered is the connection between pore and throat elements. Since throats are etched only in the model plate and are of shallower depth of etch than pores, there is a sharp edged orifice between pores and throats which may influence the nature of the curvature of the interfaces at these positions.

Mobilization pressures for the glass micromodel were calculated using the assumed advancing and receding contact angles and the dimensions of the pores and throats measured prior to fusing (Table 5.2). For a water-wet micromodel, when the displaced phases are air, hexadecane and hexadecane/air, Eqn. 1.12b is used because the leading interfaces are in the downstream throats and the trailing interfaces are in the pore bodies. For the siliconized micromodel, hexadecane is the only displaced phase that assumes the configuration for a wetting phase in a pore-throat system, i.e. with its leading interface in the pore body and its trailing interface in the upstream throat (Eqn. 1.13). The other two displaced phases, air and hexadecane/air, behave differently in the siliconized micromodel, primarily because the free gas phase has the tendency to occupy the larger spaces (i.e. pores). Air is separated from water by hexadecane because the hexadecane-air interfacial tension is less than the hexadecane-water interfacial tension, therefore, the air bubble remains in the pore spaces surrounded by a layer of hexadecane.

Table 5.2 A comparison of the water-wet and oil-wet glass micromodel systems from the difference of the cosines of the advancing and receding contact angles.

Notes : 1) Water is the displacing phase in all cases.
2) Assumptions made : Advancing and receding contact angles are the same in the glass micromodel experiments as in the capillary tube experiments.
3) For the displaced phase Hexadecane/Air, only the advancing and receding contact angles between Hexadecane and water are used in the calculation of δ.
4) The mobilization pressures (ΔP) given are based on the assumed advancing and receding contact angles and the dimensions of the micromodel measured prior to fusing.

Water-wet Micromodel (Pressures calculated from Eqn. 1.12b)

Displaced Phase	θ_R	cos θ_R	θ_A	(cos θ_A)/β	$\delta_{water\text{-}wet}$	ΔP (Pa)
Air	4.4	0.9971	6.7	0.3370	0.6601	847.3
Hexadecane	5.2	0.9959	15.1	0.3276	0.6683	450.5
Hexadecane/Air†	6.2	0.9942	15.7	0.3266	0.6675	779.0

Siliconized ("Oil-wet") Micromodel (Pressure calculated from Eqn. 1.13)

Displaced Phase	θ_R	(cos θ_R)/β	θ_A	cos θ_A	$\delta_{oil\text{-}wet}$	ΔP (Pa)
Hexadecane	126.7	-0.2028	157.4	-0.9232	0.7204	485.6

(Air and Hexadecane/Air do not assume the same configuration as Hexadecane in the siliconized micromodel)

ε (Water/Hexadecane) 1.08

Where $\beta = (r_p / r_t)$; aspect ratio

$\delta = (\cos \theta_R - \cos \theta_A)$

$\varepsilon = (\delta_{oil\text{-}wet}) / (\delta_{water\text{-}wet})$

† Air enclosed in a "skin" of hexadecane while being mobilized ($\gamma_{og} + \gamma_{ow}$ = 64.89 dynes/cm).

The only displaced phase which is comparable from water-wet to oil-wet (i.e. siliconized micromodel) is hexadecane. From Table 5.2, the dimensionless ratio (ε) of the difference of the cosines of the receding and advancing contact angles for oil-wet ($\delta_{oil\text{-}wet}$) and water-wet ($\delta_{water\text{-}wet}$) is 1.08. Based on measured pressures, ε for hexadecane is 1.66.

When mobilization pressures are calculated without including the assumed advancing and receding contact angles, the pressures do not differ greatly from those pressures calculated with the inclusion of the contact angles. The small changes in pressure suggest that, although wettability may contribute to an increase in the pressure required for mobilization, its magnitude is small when compared to that contributed by pore geometry.

Pore geometry has the effect of changing the curvature of the interface when the size of the constriction diminishes in relation to the pore size. Therefore, as aspect ratio increases, pore geometry progressively influences mobilization pressure to a greater extent. When a completely nonwetting phase or a completely wetting phase is being mobilized, the pressure depends on the following factors; the aspect ratio (or pore-to-throat size ratio) of the system, the volume and position of the phase in the pore-throat couple, and the advancing and receding contact angles associated with the interfaces. When an intermediate wetting phase ($\theta_E \sim 90°$) is being mobilized, the position of the displaced phase and the surface roughness of the system take precedence since the interface curvature will vary depending on where the three phase line makes contact with the solid surface. If one of the interfaces is positioned such that the interface is normal to the direction of fluid flow, no pressure can be sustained across it.

Another major factor which influences mobilization pressure is the

volume of the phase that is present. If a phase is nonwetting and occupies several pores and throats, then the connectivity of the phase depends on the aspect ratio of the pores and throats. Li and Wardlaw (1986) indicate that, for a contact angle $\theta \sim 0°$, the critical aspect ratio for snap off is ~ 1.5. Therefore, a nonwetting phase is likely to snap off into discontinuous singlets, each occupying a single pore.

The presence of a gas phase involves further complication with regard to its volume and compressibility. If, as mobilization pressure for a discontinuous oil/gas bubble increases, the gas portion of the bubble is compressed, then the total bubble occupies a smaller volume in the pore/throat couple, which alters the curvature of the interfaces. Compression of the gas phase may allow the entire bubble to have a greater resistance to fluid flow as the bubble adjusts to increasing pressure.

In both water-wet and oil-wet systems, when the combined hexadecane/air are the displaced phases, much of the excess hexadecane is mobilized at the lower mobilization pressure for hexadecane, leaving behind an air bubble with a thin surrounding layer of hexadecane. This implies that a bank of hexadecane will form ahead of the air/hexadecane layer which will reconnect previously isolated hexadecane blobs.

Novosad (1987) used the term mobility reduction factor (MRF) to describe the effectiveness of foam forming surfactants in diminishing gas mobility. MRF is given as the ratio of pressure drops resulting from the simultaneous flow of gas and liquid in the presence and absence of surfactant in the liquid phase. We adopt this term to refer to the ratio of pressures associated with the mobilization of hexadecane in the presence and absence of an immiscible gas phase. The MRF for the water-wet micromodel is 2.01; for the oil-wet micromodel, the MRF is 1.18.

5.3 Comparison and significance of results

From the experiments in a capillary tube and in a glass micromodel, it appears that pore geometry has a greater influence on mobilization pressures than does wettability, at least for the two media examined. This must, however be considered carefully in view of the effect wettability has on the position of the wetting (nonwetting) phase within the micromodel. In capillary tubes, contact angle hysteresis is the only factor that determines displacement pressure, resulting in pressure gradients being 7 to 12 times greater in oil-wet systems than in water-wet systems. In glass micromodel experiments reported here, the only system where the mobilization pressure for oil-wet conditions is greater than that for water-wet conditions occurs when hexadecane is the displaced phase. Hexadecane is about 1.66 times more difficult to mobilize under oil-wet conditions than under water-wet conditions.

Direct comparisons between experiments in the capillary tubes and the micromodel are not possible due to the difference in radii and pore geometry of the two porous media. In the capillary tube system, wettability is the only influence on mobilization pressure. In the glass micromodel system, additional factors, which include pore geometry, volume of the bubble and position of the bubble affect mobilization pressures. It appears that a large part of the magnitude required to mobilize a displaced phase is due to pore geometry with wettability effects being relatively minor.

5.4 Discussion of error

A complete analysis of the errors involved in the measurement of pressures from the various methods of testing (critical tilt angles, volumes of water added, difference in elevation of water reservoirs, and contact angle

measurements) is presented in Appendix A.3. The experiments performed in this study have two types of errors. The first is that of the estimated error in the primary measured quantity; the second, the error which accompanies those quantities that are calculated from the uncertain primary measurements. For example, the measurement of the critical angle of tilt for mobilization of phases in water-wet capillary tubes has an estimated error of $\pm$ 0.5 degree. However, calculation of the mobilization pressure (Eqns. 3.1, 3.2 or 3.3) also requires that the lengths of the different displaced phases and their respective densities be used in the equations. These other variables introduce their own errors into the computation. This propagation of error can be determined by applying appropriate rules when dealing with calculated values.

From error analysis, the precision of the various methods can be determined and are given in Table 5.3. Of interest is the large error associated with pressures computed from measured contact angle hysteresis, compared to the direct measurement methods (critical tilt angle, volume added and difference in elevation). For advancing and receding contact angles displaying very small hysteresis (such as air in a water-wet tube) or for angles near 90° (for example, air in an oil-wet tube), appreciable error propagates from the estimated error in the primary measured quantity (the measurement of the height of the meniscus, h, discussed in Appendix A.2). This does not make these quantities invalid but merely indicates the limitations in precision. The mobilization pressures measured directly and indirectly for capillary tube experiments are in reasonable agreement when the precision of the final values are considered.

Table 5.3 Estimation of the precision of the direct and indirect measurements of mobilization pressures in the capillary tube and glass micromodel experiments (Refer to Appendix A.3 for a listing of the errors estimated for primary measured quantities).

Capillary Tube Experiments

	Water Wet Capillary Tubes (Pressures given in Pa)		Oil Wet Capillary tubes (Pressures given in Pa)	
Phase (method)	Measured (tilt angle)	Contact Angle (θ_A and θ_R)	Measured (buret volume)	Contact Angle (θ_A and θ_R)
Air	1.85 ± 0.07	1 + 3 (-1)†	40 ± 2	40 + 90 (-40)†
Hexadecane	6.6 ± 0.3	5 ± 2†	49 ± 5	60 ± 20†
Hex/Air	8.5 ± 0.5	7 ± 6†	52 ± 6	60 ± 20†

Glass Micromodel Experiments

	Water Wet Micromodel (Pressures given in Pa)	Oil Wet Micromodel (Pressures given in Pa)
Phase (method)	Measured (elevation difference)	Measured (buret volume)
Air	600 ± 10	500 ± 30
Hexadecane	360 ± 10	600 ± 50
Hex/Air	720 ± 10	700 ± 90

† The large anomalous errors associated with mobilization pressures calculated from measured contact angles is very apparent for advancing and receding contact angles displaying very small hysteresis (for example, air in a water-wet capillary tube) or for angles near 90° (for example, air in an oil-wet capillary tube).

Chapter 6 Conclusions

6.1 General Statement

The capillary tube and glass micromodel experiments were performed in order that fluid-fluid interactions could be observed at the microscopic level under well controlled conditions with respect to both fluids and porous media. Results obtained from experiments in the cylindrical capillary tubes include :

1) the mobilization of the wetting phase requires a greater pressure gradient than for the mobilization of a nonwetting phase by a factor of about 7 to 12 times.
2) the mobilization pressure is a function of contact angle hysteresis; the larger the hysteresis, the larger the required pressure drop for mobilization.
3) when oil is the phase to be displaced in an oil-wet tube, the higher intrinsic contact angle associated with this system results in a large contact angle hysteresis compared to oil in a water-wet tube;
4) because pressure is due to advancing and receding contact angle hysteresis only, the mobilization pressure depends only on the number of interfaces present and the hysteresis associated with each pair of interfaces, therefore pressures are additive and subtractive as seen on the pressure profiles.

Experiments in a glass micromodel included the effects of pore geometry as well as wettability on mobilization pressures. In the micromodel, the wetting and nonwetting phases assumed characteristic positions within the pore-throat system. The nonwetting phase preferentially occupied the larger elements of the micromodel (i.e. pores) and the wetting phase, the smaller elements (i.e. the throats). The configuration of a discontinuous blob of nonwetting phase about

to undergo mobilization, has its leading interface in the downstream throat and its trailing interface in the pore body. The configuration for a discontinuous blob of wetting phase is opposite from that described above, with leading interface in the pore and trailing interface in the throat. The conclusions that are drawn from the glass micromodel experiments are :

1) mobilization pressures are a function of the pore geometry, the volume of displaced phase present, the position of the blob in the pore-throat couple, the interfacial tension, the advancing and receding contact angles.
2) the magnitude of resistance offered by a bubble as it is forced through a constriction is far greater than that caused by contact angle hysteresis.
3) mobilization pressures will increase with increasing aspect ratio (i.e. pore-to -throat size ratio).
4) an intermediate wetting phase (i.e. $\theta \sim 90°$) is capable of sustaining a finite pressure in a converging-diverging system depending on the position of the interfaces within the pore-throat couple; where the three phase line rests on a surface that is not normal to the axis of flow, interface curvature is present.
5) the wetting phase (hexadecane in the oil-wet micromodel) requires a greater pressure gradient to mobilize than the nonwetting phase (hexadecane in the water-wet micromodel); the magnitude of the mobilization pressure is about 1.66 times greater for the wetting phase than the nonwetting;
6) the higher mobilization pressure associated with air and hexadecane/air in the water-wet micromodel compared with hexadecane in the water-wet micromodel results from the larger interfacial tensions associated with the presence of air; for water against air, γ is 71.37 mN/m; for water against hexadecane/air, γ is the sum of the interfacial tensions for water against hexadecane and hexadecane against air, 64.89 mN/m, while for water

against hexadecane, γ is 37.48 mN/m.

7) the presence of air in an oil-wet micromodel influences the position of the combined hexadecane/air bubble since air is clearly the nonwetting phase and will occupy the large elements (i.e. the pores); air is separated from water by hexadecane because the hexadecane-air interfacial tension is less than the hexadecane-water interfacial tension. This alters the configuration observed when the displaced phase is hexadecane alone;
8) the mobilization pressures for air and hexadecane/air in both a water-wet and oil-wet micromodel are nearly of the same magnitude; this results because they assume very similar configurations, with the leading interface in the downstream throat and the trailing interface in the pore body;
9) the effects of wettability and pore geometry are difficult to separate quantitatively because the position and configurations of the displaced phases, whether wetting or nonwetting depend to a large extent on the wettability of the system.

6.2 Application to WAG process and immiscible flooding

Hydrocarbon miscible gas flooding is one of the prefered enhanced oil recovery processes currently being utilized in Alberta. The basic advantages of hydrocarbon miscible floods are : the nearly complete microscopic displacement efficiency in recovering residual oil, the abundance of large, available quantities of natural gas liquids (NGL's) and liquid petroleum gases (LPG's) and many light to medium gravity oil reservoirs that are presently in a state of production decline making them potential candidates for gas miscible flooding.

Limitations to the efficiency of miscible displacement processes result

from the low density and viscosity of the solvent and chase-gas bank, and the possible shielding of residual oil by water introduced during previous waterflooding. Viscous fingering may develop at gas-solvent and solvent-oil interfaces and sweep efficiency may be low. Because the solvent and chase gas are less dense than the oil being displaced, gravity segregation occurs and solvent may override the oil bank. The low viscosity and high relative permeability of the injected solvent and chase gas give it a high mobility, which causes viscous fingers to penetrate the oil bank. This may be controlled by a water-alternating-gas (WAG) injection scheme. Instead of a continuous injection of chase gas, the chase gas is alternated with water (either produced or fresh) for the purpose of decreasing mobility of gas and solvent and stabilizing the flood front.

The application of the results of this study lies in this area. When water and gas are alternately injected, the two phases are immiscible with each other, therefore many fluid-fluid interfaces are formed during displacement. These interfaces retard the flow of fluid through the rock-pore system ("Jamin effect").

From this study, the following inferences can be made :

1) the resistance to flow increases with increasing aspect ratio for aspect ratios of less than about 7 and, for larger ratios, resistance increases only slightly.
2) reservoir wettability does not seem to influence the mobilization pressures of the displaced phase appreciably when the gas is present as a free phase.
3) the mobilization pressures for the oil/gas phase is larger than that for oil by itself and, therefore, excess oil is mobilized ahead of the oil/gas zone facilitating formation of a continuous bank and reconnecting isolated residual oil.
4) in the absence of gas, displacement of a wetting phase requires a higher

pressure gradient than for a nonwetting phase in the same porous medium.

5) the alternate injection of gas and water reduces the relative permeability to both fluids, thereby diminishing the mobility of the fluids.

6.3 Recommendations for future work

The experiments in this study have been limited to very simple porous media at room temperature and pressure. While recognizing that this research is limited in scope with reference to the complexities of actual reservoir pore systems, the advantages are that fluid-fluid interactions could be observed at the microscopic level and the fluid and pore variables were carefully controlled so that their effects could be determined.

To further this study, the displacement of discontinuous oil and gas phases in i) an unconsolidated sand, and ii) reservoir rock samples is proposed. Results from the current study indicate that, in two-dimensional porous media, pore geometry plays an important role in the mobilization of residual phases. A three-dimensional model provides alternate pathways to fluid flow and allows gravity segregation to occur. These phenomena can only be investigated in a more complex system such as sandpacks or reservoir core.

Tests on reservoir core are extremely useful in preparing for the application of laboratory methods on a field scale, primarily because a representative sample of the porous medium is being utilized in testing for recovery efficiency. Rock-pore systems can exhibit heterogeneity on a large or small scale, and possess surface roughness characteristics which affect permeability and contact angle hysteresis. Core tests can be performed at reservoir temperatures and pressures which are not possible with fabricated porous media, however, test conditions do not allow the direct observation of the processes involved.

References

Anderson, W.G. 1986. Wettability literature survey - Part 1 : Rock/oil/brine interactions and the effects of core handling on wettability. Journal of Petroleum Technology, 38, 1125 - 1144.

Berg, R.R. 1975. Capillary pressures in stratigraphic traps. AAPG Bulletin, 59, 939 - 956.

Caudle, B.H. and Dyes, A.B. 1958. Improving miscible displacement by gas-water injection. Trans. of AIME, 213, 281 - 284.

Chatzis, I. and Morrow, N.R. 1984. Correlation of capillary number relationships for sandstone. Society of Petroleum Engineers Journal, 24, 555 - 562.

Craig, F.F. Jr. 1971. The reservoir engineering aspects of waterflooding. Society of Petroleum Engineers Of AIME Monograph 3, Dallas, 141 p.

CRC Handbook of Chemistry and Physics, 67th Edition, 1986 - 1987. Editor in Chief, R.C. Weast. CRC Press Inc., Boca Raton, Florida.

Gardescu, I.I. 1930. Behavior of gas bubbles in capillary spaces. Trans. of AIME, 86, 351 - 370.

Gibbs, R.W.M. 1929. The adjustment of errors in practical science. Oxford University Press, London, 112 p.

Harkins, W.D. and Brown, F.E. 1919. The determination of surface tension (free surface energy), and the weight of falling drops : the surface tension of water and benzene by the capillary height method. Journal of the American Chemical Society, 41, 499 - 524.

Lenormand, R., Zarcone, C., and Sarr, A. 1983. Mechanisms of the displacement of one fluid by another in a network of capillary ducts. Journal of Fluid Mechanics, 135, 337 - 353.

Li, Y. and Wardlaw, N.C. 1986. The influence of wettability and critical pore-throat size ratio on snap-off. Journal of Colloid and Interface Science, 109, 461 - 472.

McKellar, M. and Wardlaw, N.C. 1982. A method of making two-dimensional glass micromodels of pore systems. Journal of Canadian Petroleum Technology, 21, 39 - 41.

Melrose, J.C. 1964. Evidence for solid-fluid interfacial tensions from contact angles. From the Kendall Award Symposium at the 144th Meeting of the American Chemical Society, Los Angeles, Calif., April 2 - 3, 1963, Frederick M. Fowkes, Symposium Chairman. In Contact Angle, Wettability, and Adhesion. Advances in Chemistry Series, Editor, R. F. Gould, American Chemical Society, Washington, D.C.

Melrose, J.C. and Brandner, C.F. 1974. Role of capillary forces in determining microscopic displacement efficiency for oil recovery by waterflooding. Journal of Canadian Petroleum Technology, 13, 54 - 62.

Morrow, N.R. 1974. Capillary phenomena in uniformly wetted porous media. Petroleum Recovery Institute Research Report RR - 23, Calgary, Alberta, 50 p.

Morrow, N.R. 1975. The effects of surface roughness on contact angle with special reference to petroleum recovery. Journal of Canadian Petroleum Technology, 14, 42 - 53.

Ng, K.M., Davis, H.T., and Scriven, L.E. 1978. Visualization of blob mechanics in flow through porous media. Chemical Engineering Science, 33, 1009-1017.

Novosad, J.J. and Ionescu, E.F. 1987. Foam forming surfactants for Beaverhill Lake carbonates and Gilwood sands reservoirs. Presented at the 38th Annual Technical Meeting of the Petroleum Society of CIM, Calgary, Alberta, June 7 - 10, 1987. Paper No. 87-38-80.

Purcell, W.R. 1950. Interpretation of capillary pressure data. Trans. of AIME, 189, 369 - 371.

Schwartz, A.M., Rader, C.A., and Huey, E. 1964. Resistance to flow in capillary systems of positive contact angle. From the Kendall Award Symposium at the 144th Meeting of the American Chemical Society, Los Angeles, Calif., April 2 - 3, 1963, Frederick M. Fowkes, Symposium Chairman. In Contact Angle, Wettability, and Adhesion. Advances in Chemistry Series, Editor, R. F. Gould, American Chemical Society, Washington,D.C.

Shah, D.O. 1981. Introduction from Proceedings of a Symposium on Surface Phenomena in Enhanced Oil Recovery, Third International Conference on Surface and Colloid Science, Stockholm, Sweden, Aug. 20 -25,1979. In Surface Phenomena in Enhanced Oil Recovery. Editor, D.O. Shah, Plenum Press, New York, N.Y., 874 p.

Smith, W.O. and Crane, M.D. 1930. The Jamin effect in cylindrical tubes. Journal of American Chemical Society, 52, 1345 - 1349.

Stegemeier, G.L. 1977. Mechanisms of entrapment and mobilization of oil in porous media. AIChE Symposium on Improved Oil Recovery and Polymer Flooding, Kansas City, Mo., April 12 - 14, 1976. In Improved Oil Recovery by Surfactant and Polymer Flooding. Editors, D.O. Shah and R.S. Schechter, Academic Press Inc., New York, N.Y., 578 p.

Wardlaw, N.C. 1980. The effects of pore structure on displacement efficiency in reservoir rocks and in glass micromodels. First Joint SPE/DOE Symposium on Enhanced Oil Recovery, Tulsa, OK, April 20 - 23, 1980. SPE 8843.

Wardlaw, N.C. 1982. The effects of geometry, wettability, viscosity and interfacial tension on trapping in single pore-throat pairs. Journal of Canadian Petroleum Technology, 21, 21 - 27.

Wardlaw, N.C. 1986. Rock-pore properties, image analysis and EOR. AOSTRA Progress Report , Agreement 241, Project 322A.

Wardlaw, N.C. and McKellar, M. 1981. Mercury porosimetry and the interpretation of pore geometry in sedimentary rocks and artificial models. Powder Technology, 29, 127 - 143.

Wardlaw, N.C. and Wright, W.H. 1984. Immiscible gas and waterfloods in FS2 and DS6-15 glass micromodels. Unpublished Research Contract.

Wilkinson, M.C. 1972. Extended use of, and comments on, the drop-weight (drop-volume) technique for the determination of surface and interfacial tensions. Journal of Colloid and Interface Science, 40, 14 - 26.

Appendices

A.1 Derivation of equations for mobilization pressure in capillary tube

A.2 Determination of contact angles from photographs

A.3 Analysis of Error

Appendix A.1

Derivation of equations for mobilization pressure in capillary tubes

a) Water-wet capillary tube with oil-gas bubble (Refer to Figure 3)

Capillary force holding oil-gas bubble :

$P_c = (2/r) [\gamma_{wo} \cos \theta_{Awo} + \gamma_{og} \cos \theta_{Aog} - \gamma_{og} \cos \theta_{Rgo} - \gamma_{wo} \cos \theta_{Row}]$

At the instant of mobilization, $\Delta P + P_c = 0$

Therefore, $\Delta P = - P_c$

$\Delta P = (2/r) [\gamma_{wo} (\cos \theta_{Row} - \cos \theta_{Awo}) + \gamma_{og} (\cos \theta_{Rgo} - \cos \theta_{Aog})]$ (Eqn. 1.10)

b) Oil-wet capillary tube with oil-gas bubble (Refer to Figure 4)

Capillary force holding oil-gas bubble :

Note : Because the capillary is oil-wet, θ_{Awo} and θ_{Row} are both greater than 90 degrees, therefore, $\cos \theta_{Awo}$ and $\cos \theta_{Row}$ are negative values.

$P_c = (2/r) [\gamma_{wo} \cos \theta_{Awo} + \gamma_{og} \cos \theta_{Aog} - \gamma_{og} \cos \theta_{Rgo} - \gamma_{wo} \cos \theta_{Row}]$

At the instant of mobilization, $\Delta P + P_c = 0$

Therefore, $\Delta P = - P_c$

$\Delta P = (2/r) [\gamma_{wo} (\cos \theta_{Row} - \cos \theta_{Awo}) + \gamma_{og} (\cos \theta_{Rgo} - \cos \theta_{Aog})]$ (Eqn. 1.11)

Appendix A.2

Determination of contact angles from photographs

The curvature of the capillary tube distorts all measurements which are not parallel to the longitudinal axis of the tube. The only measurement that can be made perpendicular to the longitudinal axis is the outside diameter of the tube. This outside diameter, as measured through a binocular microscope (with graticule) is 1467 μm, and can be used to calibrate measurements taken off the photographs. Because the transverse measurements are distorted, the visual contact angle seen in the tube is not the actual contact angle.

The actual contact angle can be obtained by a simple geometric relationship involving the inside diameter of the tube (b), and the height the interface makes when it forms a meniscus within the tube (h) (Figure 14). This geometric relationship gives an approximation of the angle of contact between the fluid-fluid interface and the solid surface.

$$\sin\theta = (b^2 - 4h^2) / (b^2 + 4h^2)$$

These advancing (θ_A) and receding (θ_R) contact angles can be used to calculate the mobilization pressures.

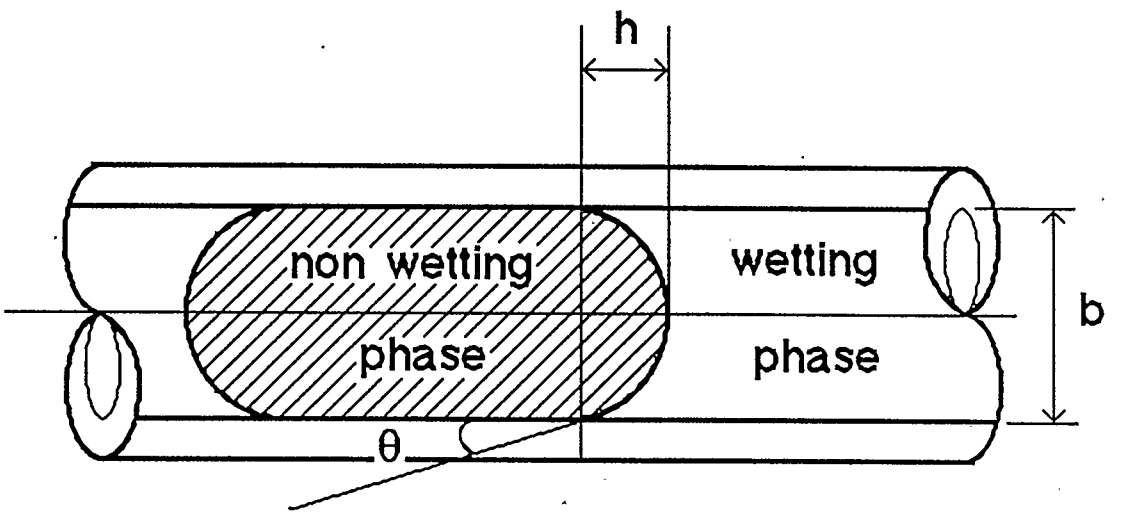

$$\text{Geometric Relationship : } \sin\theta = \frac{b^2 - 4h^2}{b^2 + 4h^2}$$

Figure 14. Geometric relationship to determine the angle the meniscus makes with the inside wall of a capillary tube of diameter b, with a meniscus height h.

Appendix A.3

Analysis of error

The estimation of error in the primary measured quantities for the different direct and indirect pressure determination methods are given below :

Direct Methods

a) Critical tilt angle method

Smallest dimension on goniometer : 1.0 degree

Error : ±0.5 degree

b) Buret volume method

Smallest dimension on buret : 0.1 ml

Error : ± 0.05 ml

c) Difference in elevation method

Smallest dimension on meter ruler : 0.1 cm

Error : ± 0.05 cm

Methods a), b) and c) also involve the use of densities, water reservoir dimensions and bubble lengths in computations.

Measured densities

Air : 0.0011 ± 0.0001 g/cm^3

Hexadecane : 0.7715 ± 0.0005 g/cm^3

Hexadecane/Air : 0.9975 ±0.0005 g/cm^3

Diameter of water reservoirs used

Inside diameter : 7.300 ± 0.005 cm

Lengths of bubbles measured from photographs

Smallest dimension on scale used : 1.0 mm

Error : 0.5 mm

Indirect Method

Contact angle determination : Calibration is accomplished by determining the outside diameter of the capillary tube and calculating the number of microns per increment of measurement on the photograph.

Diameters of the capillary tube

Inside diameter (b) : 861.66 $\pm$ 9.16 μm

Outside diameter : 1466.66 $\pm$9.16 μm

Height of meniscus (h) measured from photographs

Smallest dimension on scale used : 1.0 mm

Error : 0.5 mm

Propagation of Errors

The following are some rules used to determine the propagation of the errors in the primary measured quantities (Gibbs, 1929) :

i) The error in a sum or difference is the sum of the errors

$(A + \Delta A) + (B + \Delta B) = (A + B) \pm (\Delta A + \Delta B)$

or $(A + \Delta A) - (B + \Delta B) = (A - B) \pm (\Delta A + \Delta B)$

where A and B are the primary measured quantities, and ΔA and ΔB respectively, are the errors associated with them.

ii) The percentage error in a product or quotient is the sum of the percentage errors in the factors.

$(A + \Delta A)(B + \Delta B) = AB + A\Delta B + B\Delta A + \Delta A\Delta B$

where the required quantity, $P = AB$, such that the rest of the right hand side of the equation is the error ΔP in the product due to errors in the factors.

$\Delta P = A\Delta B + B\Delta A + \Delta A\Delta B$

The percentage error in P is therefore

$100\%(\Delta P/P) = 100\%(A\Delta B + B\Delta A + \Delta A\Delta B)/AB$

$100\%(\Delta P/P) = 100\%(\Delta A/A) + 100\%(\Delta B/B) + 100\%(\Delta A/A)(\Delta B/B)$

= percentage error in A + percentage error in B + (product of percentage errors /100)

iii) If the measurement is x with error Δx and the required quantity is y and is given by the relation : $y = f(x)$, then the error in y is : $\Delta y = f'(x)\,\Delta x$.